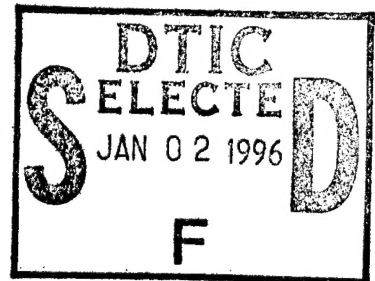


BEHAVIOR OF DAMAGED GRAPHITE/EPOXY LAMINATES
UNDER COMPRESSION LOADING



B. A. Byers

19951227 066

Boeing Commercial Airplane Company
Seattle, Washington

DISTRIBUTION STATEMENT A
Approved for public release
Distribution Unlimited

August 1980

DATA CENTER

DEPARTMENT OF DEFENSE
PLASTICS TECHNICAL EVALUATION CENTER
ARLINGTON, VIRGINIA 22204

SELECTED

44035

U.S. DEPARTMENT OF COMMERCE
National Technical Information Service

NTIS®

NASA Contractor Report 159293

BEHAVIOR OF DAMAGED GRAPHITE/EPOXY LAMINATES UNDER COMPRESSION LOADING

FINAL REPORT

(NASA-CR-159293) BEHAVIOR OF DAMAGED
GRAPHITE/EPOXY LAMINATES UNDER COMPRESSION
LOADING Final Report, Jan. 1978 - Dec. 1979
(Boeing Commercial Airplane Co., Seattle)
61 p HC A04/MF A01

N82-32420

Unclassified
CSCL 11D G3/24 31524

BRUCE A. BYERS
BOEING COMMERCIAL AIRPLANE COMPANY
P.O. BOX 3707, SEATTLE, WA 98124

CONTRACT NAS1-15107
AUGUST 1980



National Aeronautics and
Space Administration

Langley Research Center
Hampton, Virginia 23665
AC 804 827-3966

Accession For	
NTIS	CRA&I
DTIC	TAB
Unannounced	
Justification _____	
By _____	
Distribution / _____	
Availability Codes	
Dist	Avail and/or Special
A-1	

REPRODUCED BY
NATIONAL TECHNICAL
INFORMATION SERVICE
U.S. DEPARTMENT OF COMMERCE
SPRINGFIELD, VA. 22161

1. Report No. CR-159293	2. Government Accession No.	3. Recipient's Catalog No.	
4. Title and Subtitle Behavior of Damaged Graphite/Epoxy Laminates Under Compression Loading		5. Report Date August 1980	
7. Author(s) B. A. Byers		6. Performing Organization Code	
9. Performing Organization Name and Address Advanced Structures Boeing Commercial Airplane Company P.O. Box 3707 Seattle, Washington 98124		8. Performing Organization Report No. D6-48975	
12. Sponsoring Agency Name and Address National Aeronautics and Space Administration Washington, D. C. 20546		10. Work Unit No.	
11. Contract or Grant No. NASI-15107-Task 3			
13. Type of Report and Period Covered Final Report Jan. 1978-Dec. 1979			
14. Sponsoring Agency Code			
15. Supplementary Notes Langley Technical Monitor: Marvin D. Rhodes			
16. Abstract <p>(2) An experimental program was conducted to evaluate the influence of three different resin systems on the damage tolerance of graphite/polymer laminates. Testing consisted of both static compression and cyclic compression evaluation of 10.2- by 15.2- by 0.5-cm (4- by 6- by 0.2-in) laminates with circular holes, simulated delaminations, and low-velocity impact. Damage growth under steadily increasing compression and cyclic compression loading was monitored. Damage size and impact-induced failures for the three materials were compared. Of the three material systems evaluated, the one most tolerant to impact damage exhibited the least delamination within the cross section due to impact, the highest transverse tension strain to failure, and the largest crack opening force, as determined from double-cantilever-beam tests.</p> <p style="text-align: right;">Author</p>			
17. Key Words (Suggested by Author(s)) Composite, compression, impact damage	18. Distribution Statement		
19. Security Classif. (of this report) Unclassified	20. Security Classif. (of this page) Unclassified	21. No. of Pages 69	22. Price

FOREWORD

This document is the final technical report on research into damaged graphite/epoxy laminates executed in response to the statement of work for Contract NASI-15107, Task 3, "Durability and Damage Tolerance of Composite Structure Suitable for Commercial Aircraft." The work was conducted from January 1978 through December 1979. Marvin Rhodes of Langley Research Center, Hampton, Virginia, was the NASA technical monitor for the contract.

Many individuals within Boeing contributed to the acquisition of the experimental data presented in this report. Lee Shahwan coordinated specimen fabrication and inspection. Randy Coggeshall performed all the static tests, and Gary Fanning all the fatigue tests. Experimental moire' fringe support was supplied by Raymond Petit and Burke Dykes. The principal investigator and author of the report was Bruce Byers. Task 3 was managed by Robert Stoecklin and John McCarty.

The International System of Units (with parenthetic U.S. equivalents) is used throughout this report.

CONTENTS

	<u>Page</u>
FOREWORD	i
1.0 SUMMARY	1
2.0 INTRODUCTION	3
3.0 SYMBOLS AND ABBREVIATIONS	5
4.0 MATERIALS AND SPECIMENS	7
4.1 MATERIALS	7
4.2 SPECIMENS	7
4.2.1 Material Property Specimens	7
4.2.2 Static and Cyclic Compression Specimens	7
5.0 APPARATUS AND TEST	13
5.1 APPARATUS	13
5.1.1 Impact Fixture	13
5.1.2 Static and Cyclic Compression Fixture	13
5.1.3 Instrumentation	13
5.2 TESTS	13
5.2.1 Material Property Tests	13
5.2.2 Impact Tests	18
5.2.3 Static Compression Tests	18
5.2.4 Cyclic Compression Load Tests	18
6.0 RESULTS AND DISCUSSION	21
6.1 MATERIAL PROPERTY TESTS	21
6.2 LOW-VELOCITY IMPACT-DAMAGE TESTS	24
6.3 STATIC COMPRESSION TESTS	24
6.3.1 Control Tests of Undamaged Specimens	24
6.3.2 Circular-Hole Specimens	27
6.3.3 Simulated Delamination Specimens	29
6.3.4 Impact-Damaged Specimens	34
6.3.5 Comparison of Results	38
6.4 CYCLIC COMPRESSION LOADING TESTS	44
6.4.1 Circular-Hole Specimens	46
6.4.2 Simulated Delamination Specimens	47
6.4.3 Impact-Damaged Specimens	51
6.4.4 Comparison of Results	51
7.0 CONCLUSIONS	59
8.0 RECOMMENDATIONS	61
9.0 REFERENCES	63

FIGURES

	<u>Page</u>
1 Material Qualification Test Specimen	8
2 Width-Tapered, Double-Cantilever-Beam Specimen	9
3 Test Specimen Configuration	9
4 Nomenclature for Specimen Numbering	11
5 Impact Fixture	14
6 Fixture for Cyclic Compression Tests	15
7 Strain Gage Locations for Static Compression Tests	16
8 Instrumentation for Dynamic Recording of Moiré Fringes	17
9 Crack Opening Force Versus Relative Crack Opening Displacement	23
10 Extent of Impact Damage From Ultrasonic Through-Transmission Scans and Compression Failure Strains	25
11 Comparison of Fracture Modes Following Low-Velocity Impact	26
12 Damage Growth in T300/5208 Circular-Hole Specimen Under Compression Loading	28
13 Compressive Failure Strain Decrease With Increasing Hole Diameter	29
14 Failure Mode Comparison of Circular-Hole Specimens	31
15 Locations of Simulated Delaminations	32
16 Delamination Growth With Increasing Load—T300/5208	33
17 Typical Delamination Growth Characteristics—T300/5208	35
18 Damage Growth in Impacted T300/5208 Specimens Under Compression Loading	37
19 Compressive Failure Strain Reduction With Increasing Impact-Energy Levels	40
20 Load Strain Responses of Laminates With Different Types of Damage	41
21 Extent of Surface Damage Prior to Compressive Failure—T300/5208	42
22 Comparison of Delamination and Impact NDI Scans and Compressive Failure Strain—T300/5208	43
23 Failure Mode Comparison of Impact-Damaged Specimens	44
24 Failure Mode Comparison of Circular-Hole, Simulated Delamination, and Impact-Damaged Specimens	45
25 Comparison of Strength, Material, and Damage for ± 45 -deg Dominated Laminate	45
26 Damage Growth Near a Circular Hole Under Cyclic Compression Loading—T300/5208	46
27 Delamination Growth Under Cyclic Compression Loading—T300/5208	48
28 Damage Growth in a Simulated-Delamination Specimen Under Cyclic Compression Loading—T300/5208	49
29 Damage Growth in an Impacted Specimen Under Cyclic Compression Loading—T300/5208	51
30 Cyclic Compression Life Trends—T300/5208	58
31 Cyclic Compression Life Trends—T300/BP907	54
32 Cyclic Compression Life Trends—T300/P1700	55

TABLES

	<u>Page</u>
1	19
2	20
3	21
4	Physical Property Evaluation of the 10- by 15.2-cm Specimens
5	22
6	Width-Tapered, Double-Cantilever-Beam Test Results
7	23
8	Undamaged Specimen Test Results
9	27
10	Circular-Hole Test Results
11	30
12	Simulated Delamination Test Results
13	36
14	Impact-Damaged Specimen Test Results
	39
	Cyclic Compression Results for Circular-Hole Specimens
	47
	Cyclic Compression Test Results for Simulated Delamination Specimens
	50
	Cyclic Compression Test Results for Impact-Damaged Specimens
	52
	Comparison of Cyclic Compression Lives by Strain Level, Material, and Specimen Type
	56
	Results of Postfailure Analysis
	57

1.0 SUMMARY

An experimental program was conducted to evaluate the influence of commercially available resin systems on the damage tolerance of graphite/polymer laminates. Such composite materials are currently being used in aircraft secondary structure components. Use of composites on wing or body components could add significantly to overall aircraft weight reduction. Expansion of composite use to major primary aircraft structures requires improvement in the damage resistance of composite materials.

Four graphite/polymer materials were purchased and their material properties evaluated. Laminate specimens were fabricated from three of the four materials for additional damage testing. Controlled damage (circular holes and simulated delamination) and impact damage were introduced into the specimens, which were then subjected to static compression and cyclic compression load tests. Some undamaged specimens underwent only static compression tests to establish a baseline for comparing damage results. Specimens were inspected for visible damage. Nonvisible (internal) damage was detected by ultrasonic through-transmission scans.

The following matrix summarizes materials tested, specimen types, and tests performed:

Testing performed	Material				
	T300/5208	T300/BP907	T300/P1700	T300/934	
Material property	•	•	•	•	
Impact (to introduce damage and establish impact levels for compression tests)	•	•	•	Properties similar to T300/5208; excluded from further testing	
Static compression	•	•	•		
Cyclic compression loading	•	•	•		
Specimen (damage) type	Number of specimens			Type of test	
	Material				
	T300/5208	T300/BP907	T300/P1700		
Circular holes	10 6	9 6	20 5	Static Cyclic	
Simulated delamination (inserts)	22 18	22 18	None None	Static Cyclic	
Low-velocity impact	12 10	12 12	25 8	Static Cyclic	
Undamaged	6 0	6 0	6 0	Static Cyclic	

Strain gages were attached to the static test specimens to verify correct load introduction and to monitor damage growth. Moiré fringe techniques were used to monitor damage growth in both the static compression and cyclic compression tests. Damage size and impact-induced failures for the three materials were compared.

Of the three materials evaluated, the one most tolerant to impact damage exhibited the least delamination from impact, the highest transverse tension strain to failure, and the largest Mode I crack-opening force.

It is recommended that material evaluation of laminates be extended to the structural level. The tougher material systems, when verified, could significantly expand the use of graphite/polymer in primary aircraft structure. Continued testing and development is necessary to substantiate the damage containment ability of composite primary structure subjected to high strain.

2.0 INTRODUCTION

With the advent of rising fuel costs, a number of Boeing and NASA sponsored programs have been initiated to improve the operating efficiency of commercial transport aircraft. One method of improving efficiency is to reduce aircraft structural weight (refs. 1 and 2). Graphite/epoxy composite materials appear to offer a high potential for reducing structural weight, and this potential has been demonstrated in selected secondary structures (refs. 3 and 4). These secondary structures, however, account for only a relatively small amount of total aircraft structural weight. Most of the structural weight resides in components such as the wing and fuselage, and the use of graphite/epoxy composites in these components is currently under investigation.

Primary structures typically have high design operational strain levels in comparison to secondary components, which are generally designed by stiffness requirements and consequently have relatively low operational design strains. Because primary structures have high design strain levels and are critical to flight safety, the damage containment capability of the material is an important consideration.

In traditional metallic structures, damage tolerance is generally associated with small cracks that are initiated by fatigue loading and must be detected during routine visual inspection before they reach a critical size. These cracks generally occur in components that are predominantly loaded in tension. In laminated composite structures, other modes of failure may be present; for example, delamination between plies of the laminate. If this occurs in components that are predominantly compression loaded, the loading may produce interlaminar forces that can cause the damage to propagate.

Investigations have shown that graphite/epoxy composites are sensitive to impact damage (refs. 5 and 6). These studies have indicated that considerable reduction in compression strength may occur due to low-velocity impact damage that is not visually detectable.

The objective of the present investigation was to evaluate the effect of damage on the compression strength of several graphite/polymer materials with different resin systems and compare the effect of material fracture characteristics and fundamental material properties on damage tolerance. The specimens were typical of laminates that may be used in the skin of a composite aircraft wing panel (ref. 7). All of the materials selected for study were commonly available commercial resin systems.

Specimens with controlled and impact damage were subjected to static and cyclic compression loads. The types of controlled damage included circular holes and thin plastic film inserts placed between selected plies to simulate delamination. Impact damage included low-velocity impact at energy levels from 6.8J (60 in-lb) to 15.8J (280 in-lb). Damage was induced by dropping a mass into a spherical impactor at rest on the specimen surface. The extent of damage for the different materials over the range of incident energy levels was evaluated. The effect of both impact and controlled damage on compression strength of the material systems was evaluated and compared to fundamental material properties.

3.0 SYMBOLS AND ABBREVIATIONS

ϵ	failure strain
δ	deflection
a/b	specimen taper ratio
h	adherend thickness
t	laminate thickness
t_d	delamination depth
d_s	delamination damage size
D	hole or delamination diameter
E	Young's modulus of adherend
G_{IC}	strain energy release rate
P	crack initiation load
N	number of cycles
R	ratio of maximum to minimum load
W	specimen width
DCB	double-cantilever beam
kip	a 1000-lb load
ksi	thousand pounds per square inch
Msi	million pounds per square inch
NDI	nondestructive inspection

SI Units of Measure

cm	centimetre
μcm	microcentimetre
Hz	hertz
J	joule
K	degrees kelvin
kg	kilogram
kN	kilonewton
mm	millimetre
N	newton

4.0 MATERIALS AND SPECIMENS

4.1 MATERIALS

Four materials were selected for evaluation:

- Narmco T300/5208
- Fiberite T300/934
- American Cyanamid T300/BP907
- U.S. Polymeric T300/P1700

The Narmco material was selected because it is widely used and a large amount of data is available. The T300/934 was chosen for its chemical and cure similarities to T300/5208. The T300/BP907 and T300/P1700 materials were chosen based on expected improved interlamina fracture toughness.

This study was conducted to aid in identifying those basic material properties that may be related to impact damage tolerance. These particular materials were selected because it was anticipated that they would be representative of classes of basic materials. The results of this study are not intended to be used for commercial endorsement or comparison of the materials tested in this investigation. Many factors in addition to damage tolerance are involved in the selection of a material system to be used for fabrication of composite structures.

4.2 SPECIMENS

4.2.1 Material Property Specimens

Typical material property specimen configurations were used for characterizing the properties of the four materials. Sketches of the tension, compression, and short-beam shear test specimens are shown in Figure 1. In addition to these test specimens, double-cantilever-beam (DCB) specimens were fabricated to measure the resistance to interlamina fracture. Initially, height-tapered DCB specimens were tested with only partial success because of poor room temperature bonding between the aluminum and graphite. A second configuration used specimens that were bonded with a 394K (250°F) cure adhesive to the aluminum adherends and machined to width-tapered DCB's, as shown in Figure 2. The 394K (250°F) cure adhesive eliminated the problems associated with the initial specimens.

4.2.2 Static and Cyclic Compression Specimens

The specimens used to evaluate the effect of damage on compression strength of the graphite/polymer materials in static and cyclic compression are shown in Figure 3. Two basic layups were evaluated in the test program. Laminate 1 was a ± 45 -deg dominated laminate that was considered representative of upper-surface wing skins both in laminate orientation and thickness. Laminate 2 was a nearly quasi-isotropic laminate and was

Identification of commercial products in this report is used to adequately describe the test materials. Neither the identification of these commercial products nor the results of the investigation published herein constitute official endorsement, expressed or implied, of any such product by either The Boeing Company or NASA.

ORIGINAL PAGE IS
OF POOR QUALITY

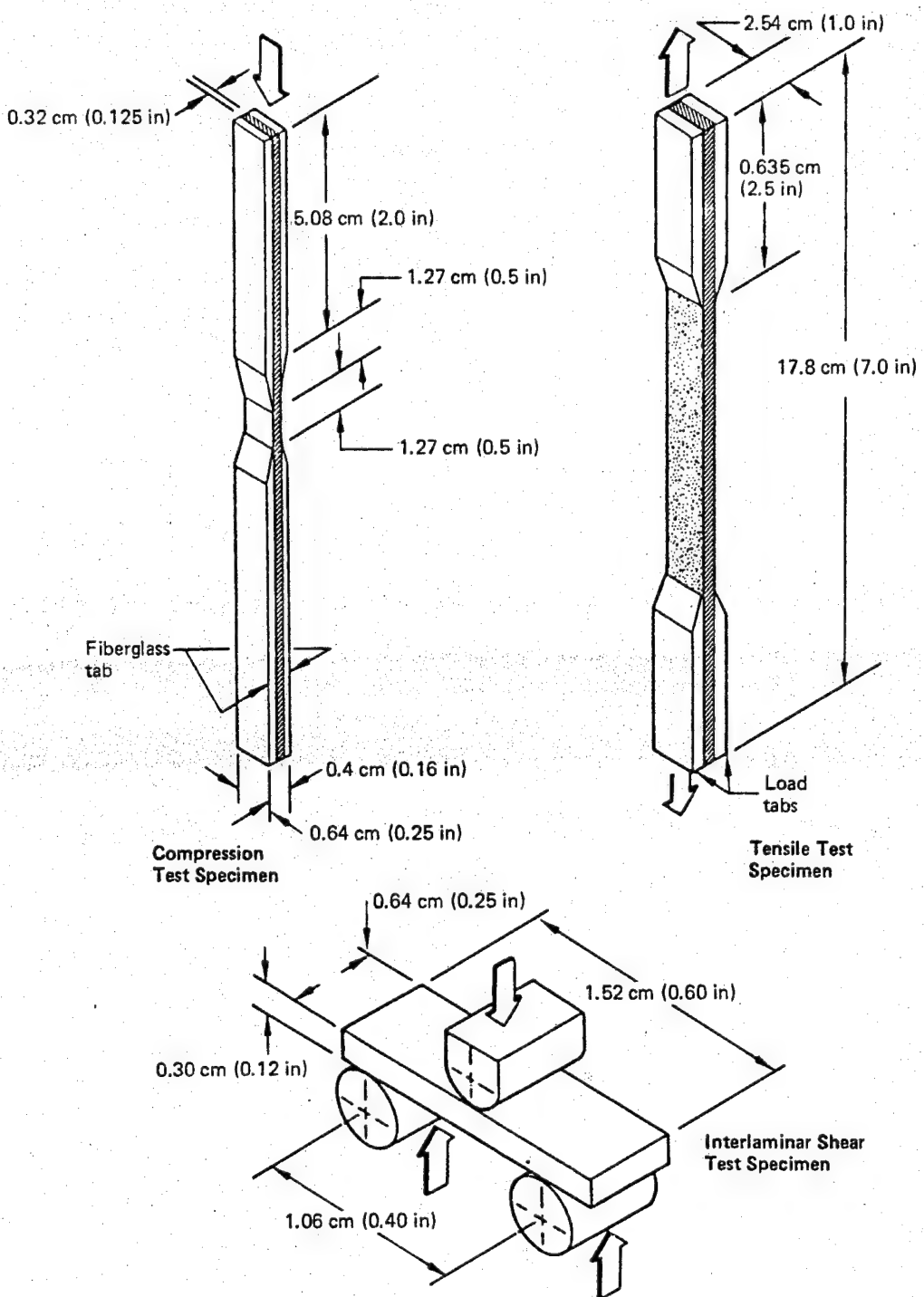


Figure 1. Material Qualification Test Specimen

**ORIGINAL PAGE IS
OF POOR QUALITY**

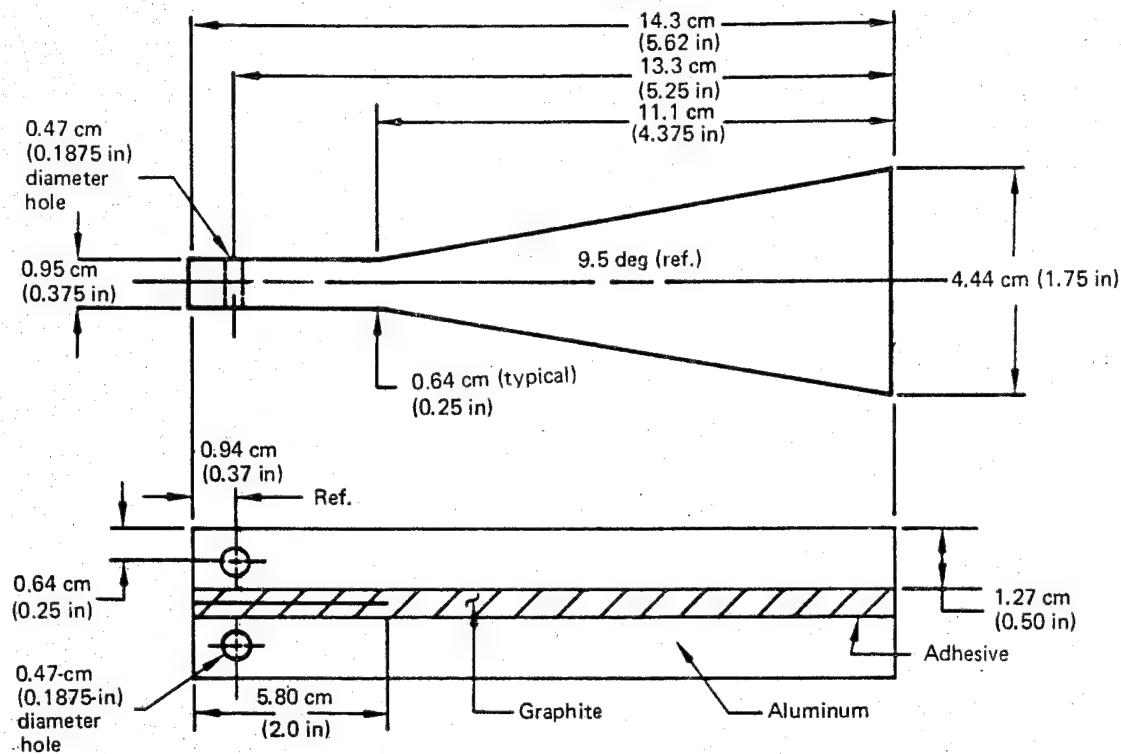


Figure 2. Width-Tapered, Double-Cantilever-Beam (DCB) Specimen

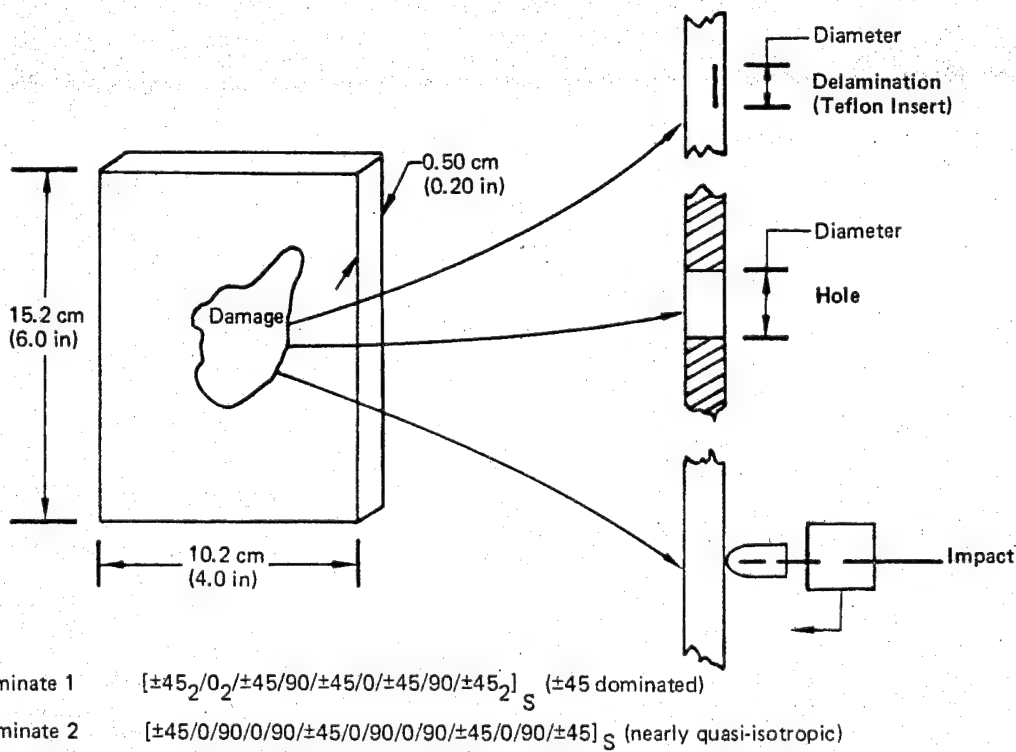


Figure 3. Test Specimen Configuration

selected as a baseline layup. Other requirements considered in the specimen selection included:

- Compression stability at strains of 10 000 $\mu\text{cm}/\text{cm}$
- Economical fabrication of the test specimens
- Edge effects
- Damage size (holes, delamination, impact) to specimen size
- Moiré fringe instrumentation access
- Load introduction uniformity

Four types of specimens—undamaged, circular-hole, simulated delamination, and impact-damaged—were tested. The circular holes in specimens ranged from 0.64 cm (0.25 in) in diameter to 3.81 cm (1.5 in) in diameter. Simulated delaminations in specimens consisted of panels with two 0.050 mm back-to-back teflon disks placed at specific locations between plies. Combinations of three disk diameters and three ply depths were tested; specific details are given in Section 6.3. All specimens were provided with a unique part number that included the following information:

- Laminate
- Material system
- Static or fatigue specimen
- Damage type
 - Undamaged
 - Impact damaged
 - Circular hole
 - Simulated delamination
- Damage size
 - Circular-hole diameter
 - Delamination diameter and ply position

The key to the specimen designation is shown in Figure 4.

The 450K (350°F) cure materials—T300/934, T300/5208, and T300/BP907—were purchased to a standard Boeing specification and processed as recommended by the material supplier.

The 10.2- by 15.2-cm (4- by 6-in) specimens were cut and machined from large flat laminate sheets. To ensure uniform load distribution, specimen ends were ground flat and parallel after machining. Teflon inserts were placed in appropriate locations during fabrication. Following cure, large panels were inspected with ultrasonic through-transmission scans. X-ray scans of simulated delamination specimens were used to check positioning and placement of strain gages.

**ORIGINAL PAGE IS
OF POOR QUALITY**

Laminate number (see figure 3)	Material	Test	Damage type	Damage size, cm (in)	Delamination depth
1	1 = T300/5208	S = Static	N = None	1 = 0.64 (0.25)	3 = 12 plies
2	2 = T300/P1700	F = Fatigue	I = Impact	2 = 1.27 (0.50)	6 = 6 plies
3	3 = T300/BP907		H = Hole	3 = 2.54 (1.00)	9 = 4 plies
			D = Delamination	4 = 3.81 (1.50)	

Figure 4. Nomenclature for Specimen Numbering

5.0 APPARATUS AND TEST

5.1 APPARATUS

5.1.1 Impact Fixture

Damage by low-velocity impact was induced in the composite laminates using the fixture shown in Figure 5. The 10.2- by 15.2-cm (4- by 6-in) specimens rested on a platform having a 7.6- by 12.7-cm (3- by 5-in) rectangular cutout, which supported the specimens along the edge. A 1.8-kg (4-lb) weight was dropped down a calibrated tube, striking a 1.6-cm (0.62-in) diameter spherical head impactor that rested on the specimen. The support, size, and thickness of the specimen gave an effect similar to dropping a tool from a few feet onto a wing skin and striking it between stiffeners. Impact energy levels and resulting damage produced in this fixture were not directly comparable with other impact-induced damage. The intent was to produce impact damage for material comparisons that were in the range of real damage threats. The cause and specific impact levels were of secondary importance.

5.1.2 Static and Cyclic Compression Fixture

Support fixtures were used for testing the 10.2- by 15.2-cm (4- by 6-in) laminates. Photographs of a typical setup, presented in Figure 6, show the specimen supported on the sides by rounded knife edges that provide lateral support to prevent specimen instability. The lateral supports are rigidly attached to the base of the fixture, thereby ensuring that the specimen is aligned perpendicular to the loading heads. Between each cyclic compression test, a strain-gaged aluminum plate "standard" was placed in the fixture to check fixture alignment.

5.1.3 Instrumentation

Back-to-back strain gages were placed in the two upper corners of the static test specimens. Gages were also placed near the circular holes and over delaminated regions when appropriate, as shown in Figure 7.

Moiré fringe techniques were used to monitor delamination growth in both the static compression and cyclic compression tests. The dynamic moiré fringe setup for cyclic compression tests is shown in Figure 8. A strobe light synchronized with the loading frequency illuminated the moiré fringes during the load cycle peak. A load cycle counter triggered the strobe and camera at selected cycle intervals.

5.2 TESTS

5.2.1 Material Property Tests

Material property tests were conducted on the four materials to establish baseline material properties. Additional tests were selected to provide a comparative basis for fracture and impact characteristics. The properties of specific interest for fracture and impact comparisons included:

- Damage growth initiation force between lamina
- Transverse strain to failure

To evaluate these properties and other resin-dependent properties, the following discriminating tests were conducted:

- Double-cantilever beam
- 90-deg tension
- Short-beam shear
- 0-deg compression strength

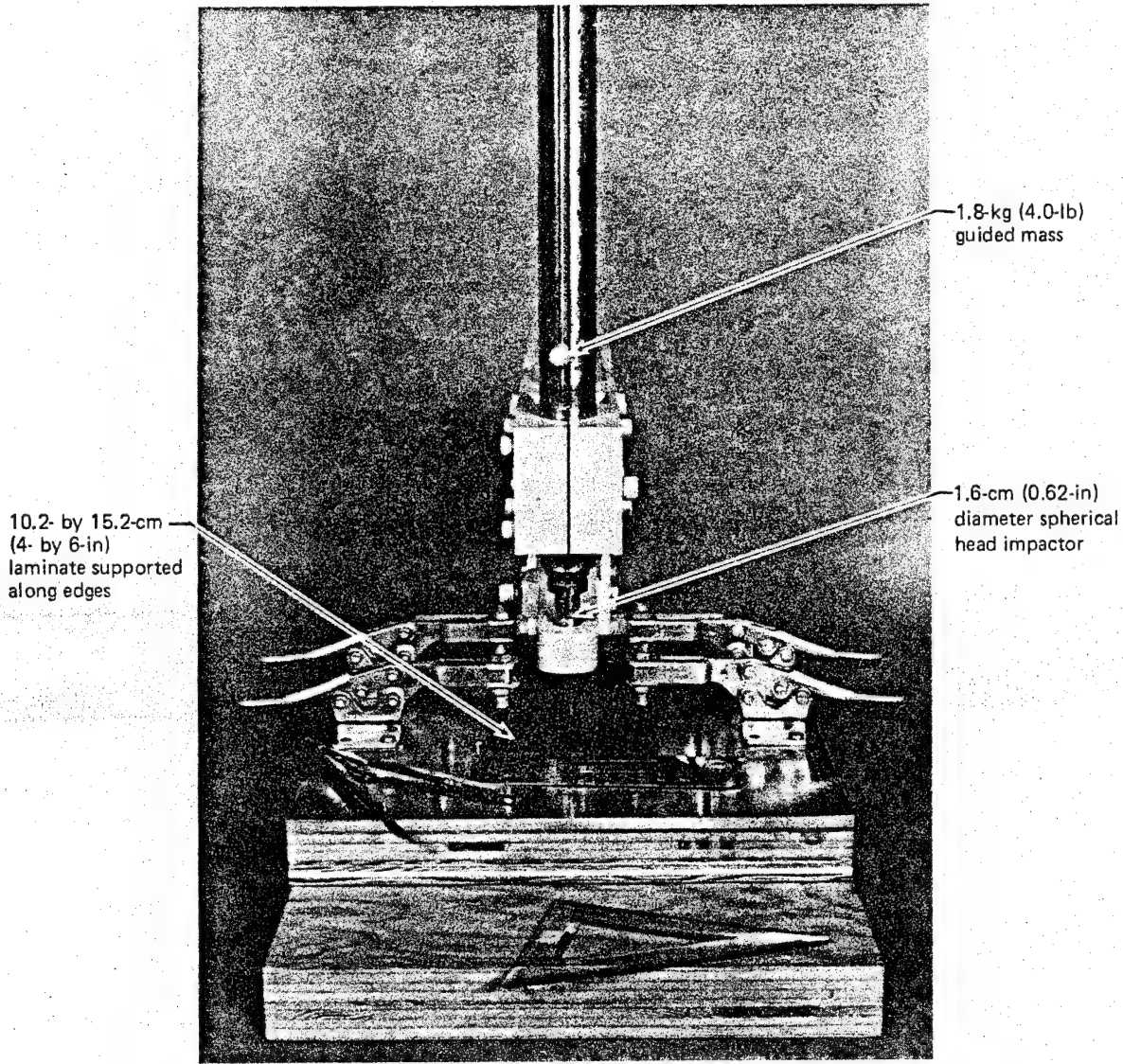
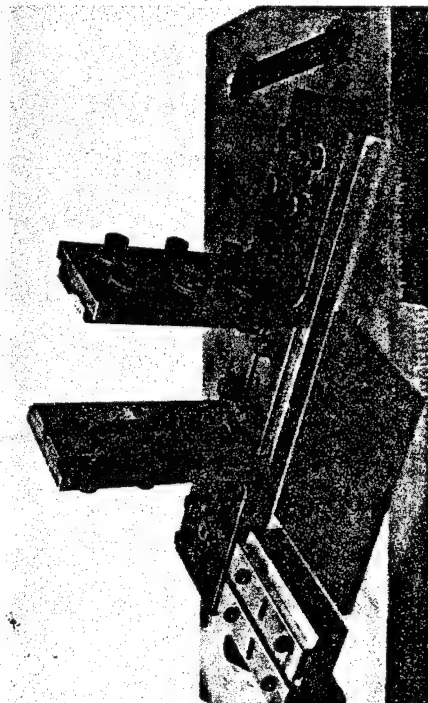
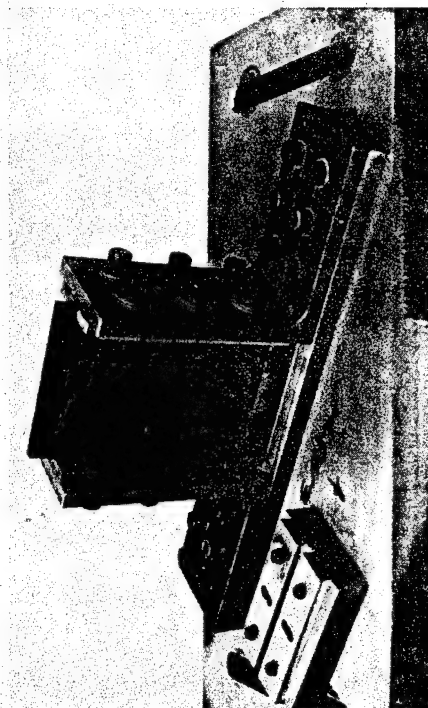


Figure 5. Impact Fixture

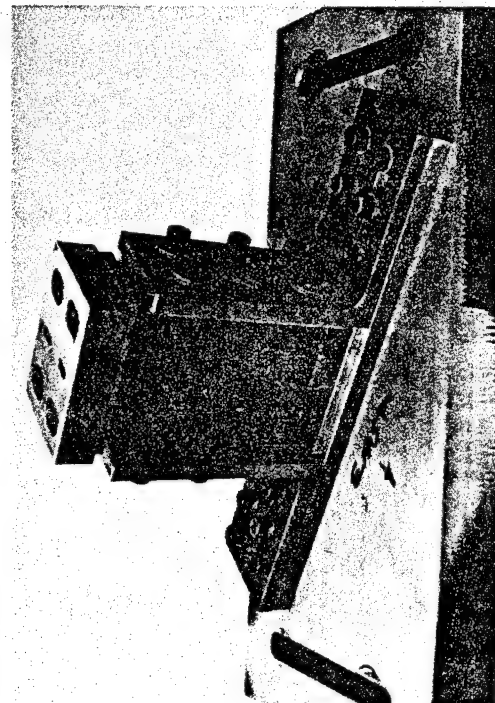
ORIGINAL PAGE IS
OF POOR QUALITY



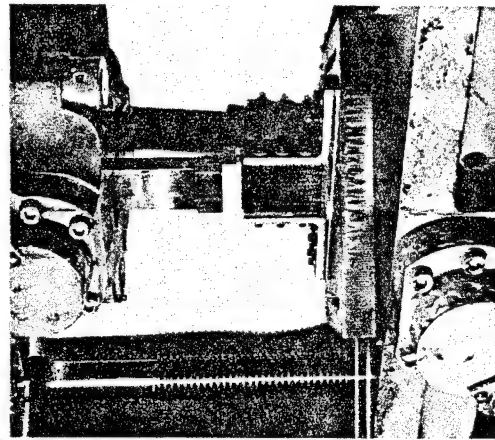
Compression test fixture.



Compression test fixture with specimen in place



Compression test fixture
with specimen ready for test



Compression fixture in test
machine

Figure 6. Fixture for Cyclic Compression Tests

ORIGINAL PAGE IS
OF POOR QUALITY

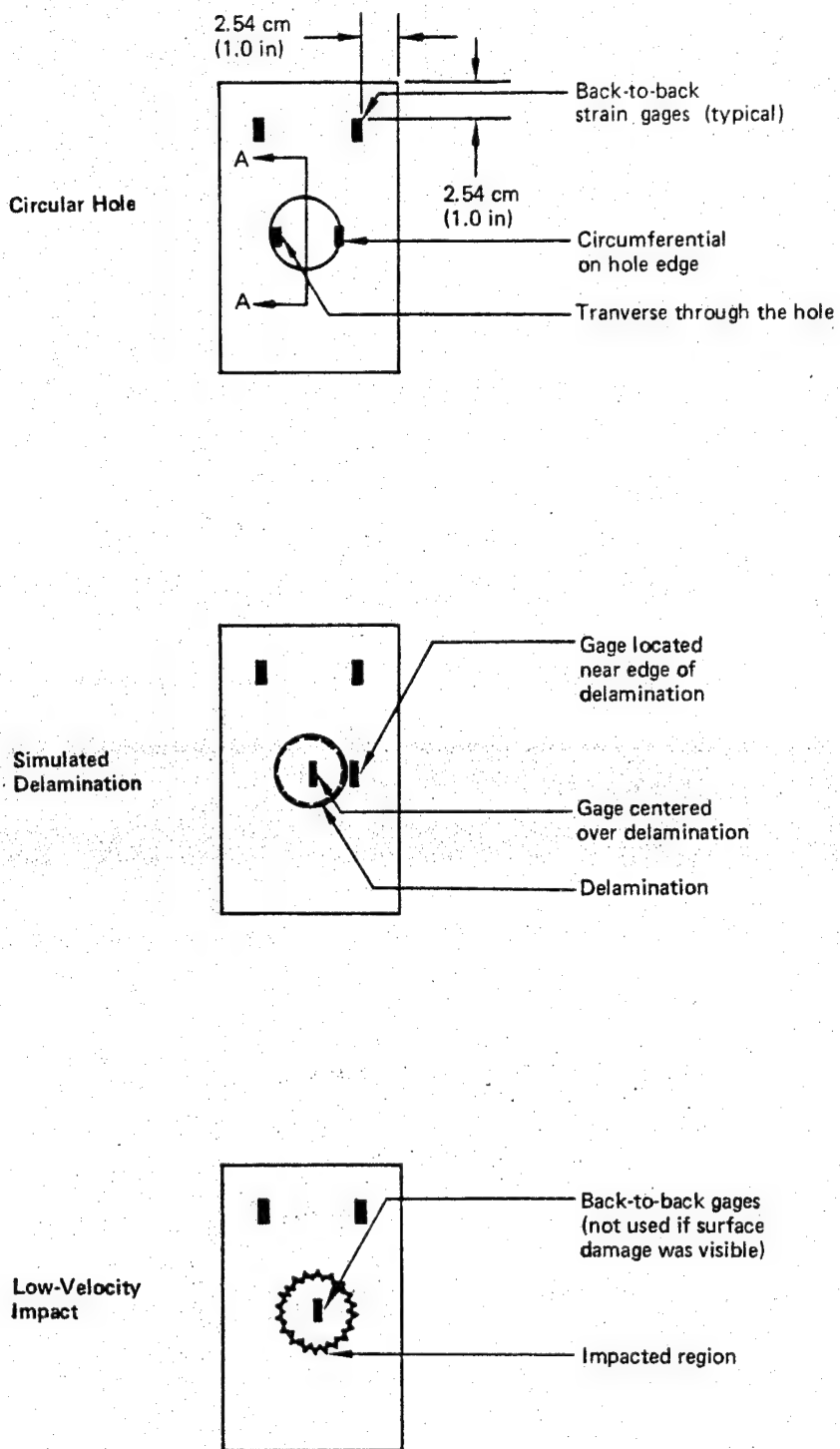


Figure 7. Strain Gage Locations for Static Compression Tests

ORIGINAL PAGE IS
OF POOR QUALITY

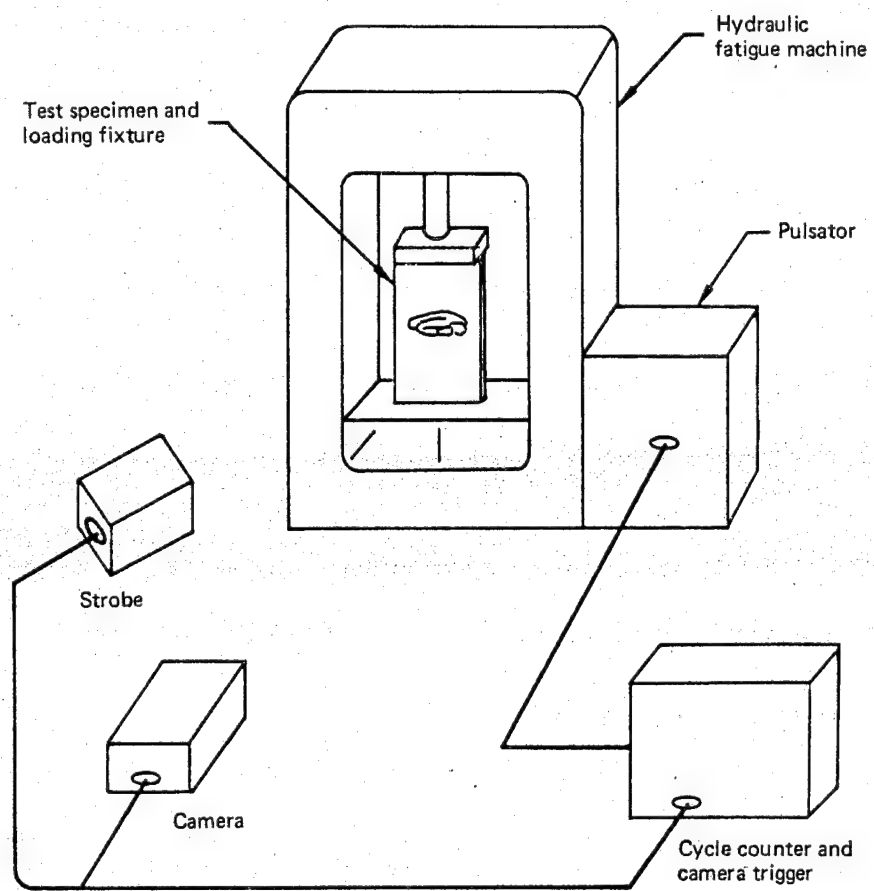


Figure 8. Instrumentation for Dynamic Recording of Moiré Fringes

5.2.2 Impact Tests

A criterion was developed for selecting impact levels for the 10.2- by 15.2-cm (4- by 6-in) laminate specimens. The primary objective was to introduce a range of impact damage that would extend from easily detectable (visible only) damage to a lower level requiring nondestructive inspection to detect any internal damage. This range varies with material systems and specimen configurations. It has been shown by numerous tests that nonvisually detectable damage can result in significant compression strength reduction (ref. 5). A second objective for selecting impact levels was to obtain static compression and cyclic compression test results for an identical level of impact for the three materials being evaluated.

5.2.3 Static Compression Tests

The complete static compression test matrix for the three material systems evaluated is shown in Table 1. Head travel and failure loads were obtained for all these specimens. Monitoring and evaluating the compression load response of the three materials and the various damage types also was accomplished during these tests. For example, specimens with delamination exhibited local instability in the region of the insert. Following instability, increasing the load resulted in slow delamination propagation. To monitor this behavior, moiré fringes and strain gages were positioned as shown in Figure 7. The specimens were loaded incrementally to monitor damage propagation.

Two specimens were fabricated for each damage size; one was fully instrumented, whereas the second was instrumented for head travel and failure load only.

5.2.4 Cyclic Compression Load Tests

In addition to the static compression tests, the influence of cyclic compression loading was also evaluated. Table 2 is the cyclic test specimen matrix. The types of laminate damage (holes, delaminations, and impact) are identical to the static test. Only the ± 45 -deg dominated laminate was selected for evaluation in the cyclic load tests, which were conducted to establish trends between cyclic compression capability for different damage types and resin systems. Cyclic strain levels were chosen based on the static test results for specific specimens.

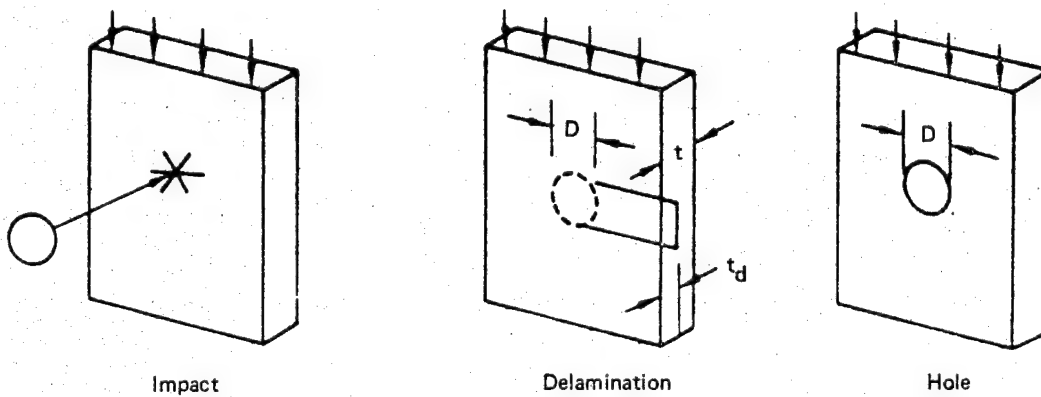
A number of duplicate specimens were tested at various cyclic compression strain levels to evaluate the effect of strain level on cyclic compression life. Specimens were cycled at 10 Hz. The initial test specimens were cycled at high strain levels. Strain levels on subsequent specimens were reduced to establish cycle-to-failure trends. One million cycles was considered a practical upper boundary on testing time for most specimens. For specimens that exceeded one million cycles, cyclic strain levels were increased to induce failure. Large differences in cyclic compression capability of specimens with various types of initial damage (holes, delamination, and impact) resulted in a broad range of test variables. The maximum cyclic compressive strain levels varied from $-2500 \mu\text{cm}/\text{cm}$ to $-8000 \mu\text{cm}/\text{cm}$. Cyclic compression lives varied from a low of 2340 cycles to a maximum of four million cycles.

The majority of fatigue specimens were not strain-gaged because of early specimen problems with strain gage reliability on specimens cycled at high strain levels. As previously discussed, dynamic recording of moiré fringes was used on a few specimens to monitor delamination growth.

ORIGINAL PAGE IS
OF POOR QUALITY

Table 1. Matrix of Static Compression Tests

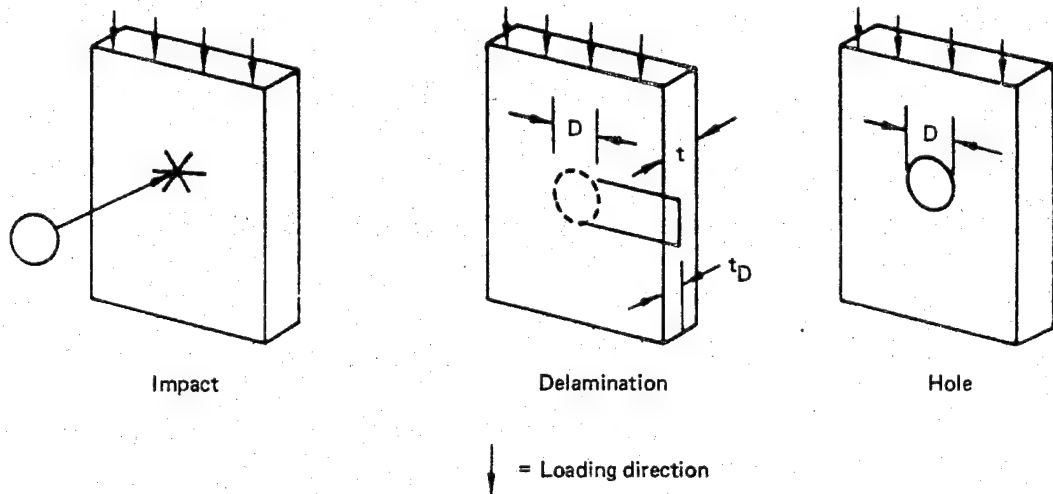
Specimen type	Specimen description	Number of specimens		
		Material		
		T300/5208	T300/BP907	T300/P1700
Circular holes	Diameter, cm (in)			
	0.64 (0.25)	4	4	4
	1.27 (0.5)	4	4	4
	2.54 (1.0)	2	1	6
Simulated delamination (inserts)	Diameter, cm (in)	Ply depth		
	1.27 (0.5)	{ 4 6 12 4 6 12 4 6 12	1 4 4 2 1 0 4 4 2	1 4 4 2 1 0 4 4 2
	2.54 (1.0)			No test conducted
	3.81 (1.5)			
Low-velocity impact	Incident energy, J (in-lb)			
	6.78(60)	4	0	5
	11.30(100)	4	2	4
	15.8 (140)	4	4	5
	21.5 (190)	0	0	5
	24.8 (220)	0	2	0
	27.1 (240)	0	0	4
	31.6 (280)	0	4	2



= Loading direction

Table 2. Matrix of Cyclic Compression Tests

Specimen type	Specimen description	Number of specimens		
		Material		
		T300/5208	T300/BP907	T300/P1700
Circular holes	Diameter, cm (in)	1.27 (0.5)	6	5
Simulated delamination (inserts)	Diameter cm (in)	Ply depth		
	1.27 (0.5)	4	6	6
	3.81 (1.5)	4	6	6
	3.81 (1.5)	12	6	No test conducted
Low-velocity impact	Incident energy, J (in-lb)	6.78 (60) 15.8 (140) 31.6 (280)	6 4 6	4 4



6.0 RESULTS AND DISCUSSION

6.1 MATERIAL PROPERTY TESTS

Table 3 summarizes material property test data for the four materials. A number of differences are evident. Resin volume content in the cured laminate is greater in the T300/BP907 and T300/P1700 laminates than in the T300/5208 and T300/934 laminates. Both the P1700 and the two-phase, rubber-modified BP907 systems exhibit less resin flow during cure than do the 5208 or 934 resin systems. Resin content for laminates of the three materials from which all the 10.2- by 15.2-cm (4-by 6-inch) specimens were machined are shown in Table 4. The resin volume percentages in Tables 3 and 4 are in close agreement. The T300/P1700 material property test results are low for compression, tension, and short-beam shear. For the graphite/epoxy materials, T300/934 exhibits slightly higher 0-deg tension strength, 0-deg compression strength, and short-beam shear strength than both T300/5208 and T300/BP907. The T300/BP907 material displays large 90-deg tension strain to failure, which is probably due primarily to better resin ductility but may also be influenced by the higher resin content.

Table 3. Material Property Tests

Prepreg	Property	T300/5208	T300/BP907	T300/P1700	T300/934
Laminate	Area weight, gm/m ² (oz/yd ²)	145 (4.30)	142 (4.21)	—	149 (4.42)
	Resin content, % weight	40.5	41.5	—	40.5
	Ply thickness, mm (mils)	0.127 (5)	0.147 (5.8)	0.142 (5.6)	0.129 (5.1)
	Resin volume, % volume	35.9	41	46	31
	Fiber volume, % volume	64.8	58	54	69
	0-deg compression modulus*	13.4 (19.4)	13.9 (20.0)	11.4 (16.6)	12.6 (18.2)
	0-deg compression strain to failure*	9830	9500	5500	13 350
	0-deg compression strength*	132.0 (190.7)	131.0 (190.0)	63.6 (92.2)	168.0 (243)
	0-deg tension modulus	15.1 (21.9)	12.1 (17.6)	11.2 (16.2)	16.8 (24.3)
	0-deg strain to failure	8890	10 740	7126	10 675
	0-deg tensile strength	142 (206)	130 (189)	77.9 (113.0)	157 (228)
	90-deg tension modulus	0.87 (1.27)	0.66 (0.96)	0.72 (1.04)	0.83 (1.21)
	90-deg tension strain to failure	4340	9770	2000	4780
	90-deg tension strength	4.31 (6.26)	6.43 (9.33)	1.59 (2.31)	3.97 (5.76)
	45-deg tensile strength	18.0 (26.2)	20.6 (30.0)	11.5 (16.7)	15.9 (23.0)
	Short-beam shear strength	11.2 (16.2)	9.10 (13.2)	7.03 (10.2)	11.4 (16.5)

*Modulus: MN/cm² (Msi)
Strength: kN/cm² (ksi)
Strain: μ cm/cm

Table 4. Physical Property Evaluation of the 10- by 15.2-cm Specimens

Specimen number	Material	Resin content, % weight	Void content, %	Fiber volume, %	Resin volume, %	Composite density, g/cm ³
11SI-4 21SN-3	T300/5208	28.1 27.7	-0.45 -0.58	64.90 65.28	35.56 35.30	1.57 1.57
13SD39-2 23SD49-2	T300/BP907	36.2 37.1	0.67 -0.45	55.35 54.96	43.98 45.49	1.51 1.52
12SI-6 22SD46-1	T300/P1700	35.5 37.6	0.18 0.18	56.2 53.8	43.6 45.8	1.52 1.50

Resin and fiber densities, g/cm³

P1700 resin: = 1.24
5208 resin: = 1.28
T300 fiber: = 1.74

A review of the material property test data showed little difference between the properties of T300/5208 and T300/934. Therefore, T300/934 was excluded from all subsequent testing because the two materials were expected to yield similar fracture toughness.

A comparative measure of the interlamina fracture toughness was obtained using the width-tapered cantilever beam. During the tests the crack opening force was monitored. Figure 9 shows typical load versus displacement curves for each of the three materials evaluated. Several interesting differences associated with the various resin systems are apparent. These included the peak load associated with interlamina fracture of the specimen and the "fracture energy" given by the area under the load versus deflection curve. These differences provide a basis for making material toughness comparisons. The T300/BP907 has considerably higher fracture toughness than T300/P1700 and T300/5208, as implied by Figure 9 and Table 5.

An attempt to determine the load under which crack growth initiated was less definitive. The loads at crack initiation shown in Table 5 were obtained from the first sudden drop in load level recorded on the load versus deflection plot. It is surmised that crack growth initiation loads are more sensitive to crack front variables than the maximum load associated with interlamina fracture.

Specimen geometry of this type has been used to obtain strain energy release rates associated with a new crack surface in adhesives. For the geometry of these specimens theoretical strain release rates, GIC, are given by

$$G_{IC} = \frac{12P^2}{Eh^3} (a/b)^2$$

where P is the crack initiation load, E is Young's modulus of the adherend, a/b is the specimen taper ratio, and h is the adherend thickness.

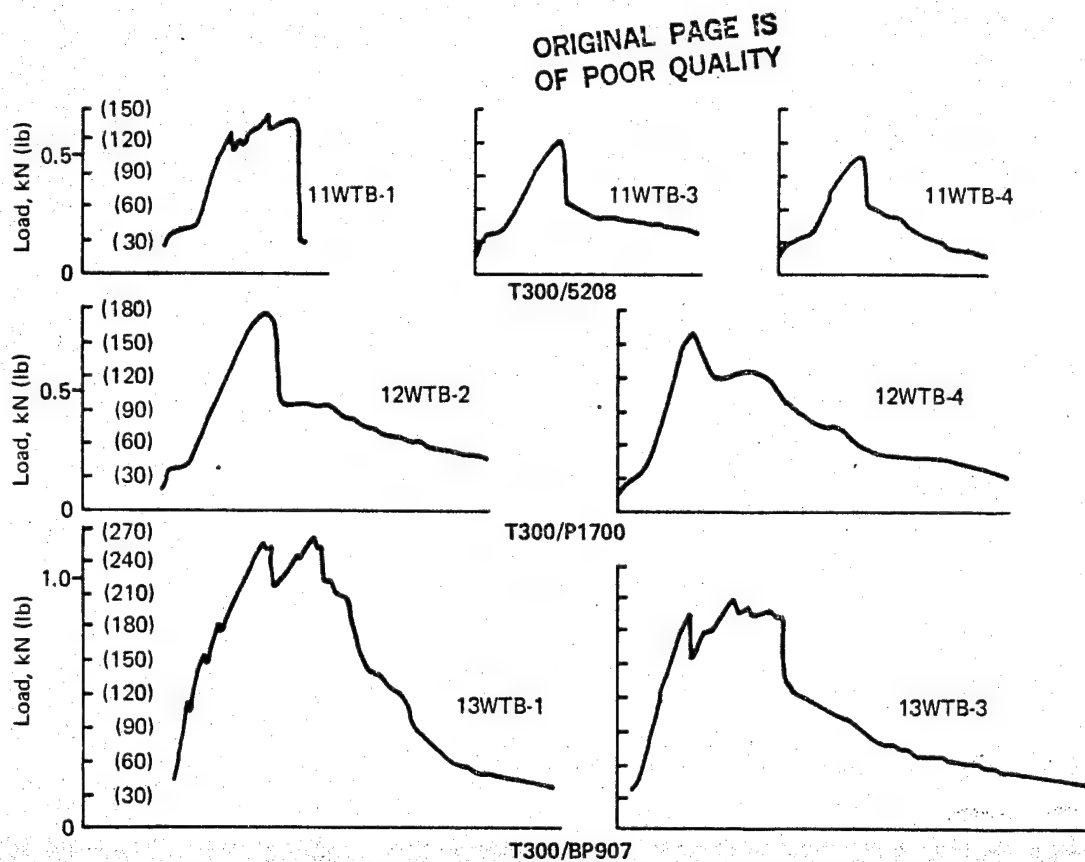


Figure 9. Crack Opening Force Versus Relative Crack Opening Displacement

Table 5. Width-Tapered, Double-Cantilever-Beam Test Results

Material	Specimen number	Initial crack length cm (in)	Crack initiation load, N (lb)	G_{IC}^* J/m ² × 10 ² (in-lb/in ²)	Maximum load, N (lb)	G_{IC}^{**} J/m ² × 10 ² (in-lb/in ²)
T300/ 5208	11WTB-1	4.3 (1.70)	563 (126.5)	2.41 (1.38)	563 (126.5)	2.41 (1.38)
	11WTB-2	4.3 (1.70)	463 (104.0)	1.63 (0.93)	463 (104.0)	1.63 (0.93)
	11WTB-3	5.1 (2.00)	552 (124.0)	2.33 (1.33)	552 (124.0)	2.33 (1.33)
	11WTB-4	2.8 (1.10)	489 (109.5)	1.82 (1.04)	489 (109.5)	1.82 (1.04)
T300/ P1700	12WTB-1	4.3 (1.70)	667 (150.0)	3.39 (1.94)	667 (150.0)	3.39 (1.94)
	12WTB-2	6.4 (2.50)	796 (179.0)	4.83 (2.76)	796 (179.0)	4.83 (2.76)
	12WTB-3	4.3 (1.70)	612 (137.5)	2.85 (1.63)	625 (140.5)	2.47 (1.71)
	12WTB-4	4.3 (1.70)	729 (164.5)	4.10 (2.34)	729 (164.5)	4.10 (2.34)
T300/ BP907	13WTB-1	4.3 (1.65)	489 (110.0)	1.84 (1.05)	1165 (262.0)	10.38 (5.93)
	13WTB-2	4.3 (1.70)	572 (128.5)	2.50 (1.43)	1098 (247.0)	9.23 (5.27)
	13WTB-3	4.3 (1.70)	881 (198.0)	5.94 (3.39)	916 (206.0)	6.43 (3.67)
	13WTB-4	4.3 (1.70)	507 (114.0)	1.96 (1.12)	1223 (274.9)	11.40 (6.51)

$$G_{IC} = \frac{12P^2}{Eh^3} \left(\frac{a}{b}\right)^2$$

* G_{IC} based on crack initiation load

** G_{IC} based on maximum load

For these specimens the range of G_{JC} varies from 1.63 N/cm (0.93 lb/in) to 11.4 N/cm (6.51 lb/in). As shown in Table 5, the G_{JC} values based on crack initiation load are similar for T300/5208 and T300/BP907. G_{JC} values based on the maximum load obtained are considerably greater for T300/BP907 than for T300/P1700 and T300/5208. Failure of these specimens involved a number of plies, not a single plane of delamination.

Because of the above experimental observations, reported values of G_{JC} associated with tests of this type require clarification on specimen geometry, laminate details, load versus deflection curves, and fracture surface definition. For material screening tests of interlaminar fracture toughness, the peak load or fracture energy is probably a more realistic toughness measure for a given specimen geometry.

6.2 LOW-VELOCITY IMPACT-DAMAGE TESTS

The 10.2- by 15.2-cm (4- by 6-inch) specimens were impacted in the fixture described previously in Section 5.1.1 at the level described in Section 5.2.2. Levels were selected that would produce barely visible damage. To evaluate internal damage, ultrasonic through-transmission scans of the impacted specimens were conducted. Figure 10 shows portions of these scans for different impact energy levels and different material systems. These representative scans reveal a number of features, including a large range in the damage threshold. As shown in the figure, the impact energy required to induce ultrasonic detectable damage in T300/BP907 is greater than that for T300/5208 and T300/P1700. Significant differences in damage size under identical impact conditions are apparent. The specimen compressive failure strains indicated in the figure are discussed in Section 6.3.

Another measure of impact damage is how the damage is distributed throughout the laminate thickness and which impact-induced fracture modes have resulted, since these may control how the laminates fail under static compression loading. Following impact, a few specimens were sectioned and photomicrographed. Results for the three material systems are shown in Figure 11. Impact-induced fracture modes differ significantly for each of the three materials. The T300/5208 material exhibits extensive delamination on many planes throughout the laminate thickness. In addition, there is considerable shattering of the delaminated layers. The T300/BP907 material exhibits less delamination, some transverse cracks, and some fiber failure on the side opposite the contact region. The T300/P1700 failures are similar in appearance to the T300/BP907; however, no fiber fracture is present. Both T300/BP907 and T300/P1700 have a larger permanent indentation (plastic deformation) under the 1.6-cm (0.6-in) spherical head impactor than the T300/5208 specimens.

6.3 STATIC COMPRESSION TESTS

6.3.1 Control Tests of Undamaged Specimens

A total of 150 static compression tests were conducted. In addition to the laminates with holes, delamination, and impact damage, 18 undamaged specimens were tested to establish a baseline for comparing damage results. The instrumentation setup, specimen stability, and loading fixture were also evaluated on these initial specimens. Test results on the undamaged specimens are shown in Table 6. The T300/BP907 specimens have the highest compression failure loads and strains, followed by T300/5208, then T300/P1700. The ± 45 -deg dominated laminates exhibit lower compression failure loads but greater failure strains than the nearly quasi-isotropic laminates in both T300/BP907 and T300/5208 (see fig. 3).

ORIGINAL PAGE IS
OF POOR QUALITY.

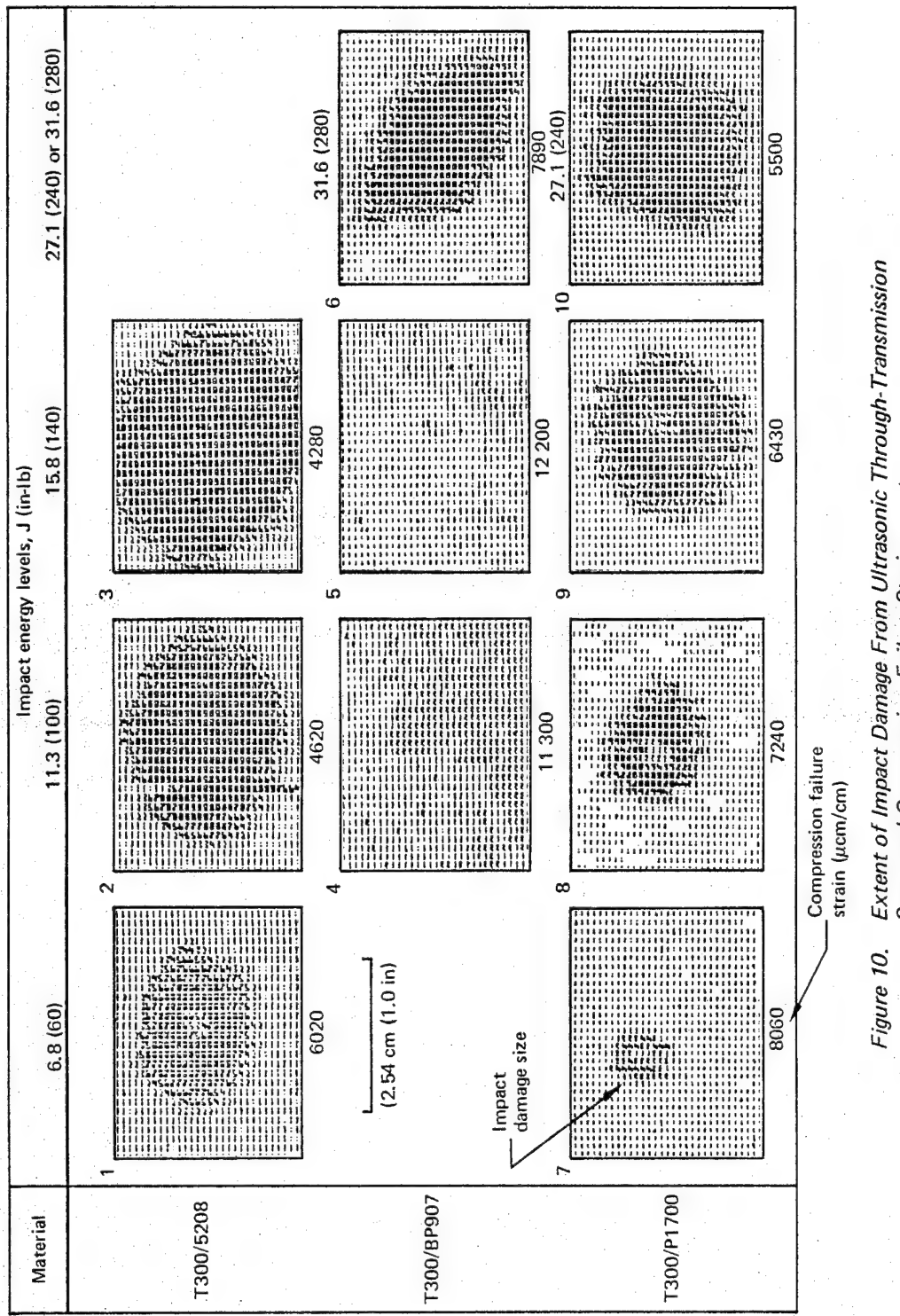


Figure 10. Extent of Impact Damage From Ultrasonic Through-Transmission Scans and Compression Failure Strains



- T300/5208
 - Impact = 15.8J (140 in-lb)
 - Delamination
 - Transverse cracks
 - Internally shattered

- T300/BP907
 - Impact = 31.6J (280 in-lb)
 - Delamination
 - Fiber fracture
 - Transverse cracks

- T300/P1700
 - Impact = 15.8J (140 in-lb)
 - No damage under impactor
 - Transverse cracks

Figure 11. Comparison of Fracture Modes Following Low-Velocity Impact

Table 6. Undamaged Specimen Test Results

Material	Specimen number	Failure load, kN (kip)	Failure strain, μcm
T300/5208	11SN-1	187.2 (42.10)	9 960
	11SN-2	166.3 (37.40)	8 825
	11SN-3	201.9 (45.40)	10 554
	21SN-1	180.2 (40.50)	8 233
	21SN-2	216.4 (48.65)	9 112
	21SN-3	206.4 (46.40)	8 613
T300/BP907	13SN-1	214.4 (48.20)	12 429
	13SN-2	195.7 (44.00)	10 592
	13SN-3	240.2 (54.00)	13 300
	23SN-1	257.9 (58.00)	10 866
	23SN-2	253.5 (57.00)	10 337
	23SN-3	250.4 (56.30)	10 400
T300/P1700	12SN-1	165.0 (37.10)	8 233
	12SN-2	172.5 (38.80)	8 825
	12SN-3	160.1 (36.00)	8 050
	22SN-1	142.3 (32.00)	5 422
	22SN-2	133.4 (30.00)	5 192
	22SN-3	145.0 (32.60)	5 680

Failure loads and strains in the T300/P1700 nearly quasi-isotropic laminate were very low. Test results and failure modes for this material were erratic in relation to the T300/5208 and T300/BP907 results. The processing maturity of this thermoplastic material system is not as well developed as the 450K (350°F) graphite/epoxy systems. This should be recognized when making material comparisons using the test data for this material.

Failure modes of the undamaged T300/5208 specimens were characterized by a few planes of extensive delamination over a major portion of the specimen. The T300/BP907 specimens exhibited some delamination with a predominant shear failure mode.

6.3.2 Circular-Hole Specimens

Figure 12 presents representative experimental data for a circular-hole specimen of T300/5208. The moiré fringe contours indicate that surface delamination can precede specimen failure. Strain gages placed near the edge of the hole (gage 5) provided a measure of the strain concentration. The measured maximum compression strains on the hole edge were in the 16 000-to 20 000- $\mu\text{cm}/\text{cm}$ range and produce a typical strain concentration value of 2.80. Large transverse (through-the-thickness) tensile strain on the inside surface of the hole was also recorded (gage 6). These strains reflect the large out-of-plane Poisson ratios.

Figure 13 and Table 7 summarize circular-hole tests. The recorded failure strain is based on the average strain of the back-to-back strain gages in the specimen corners.

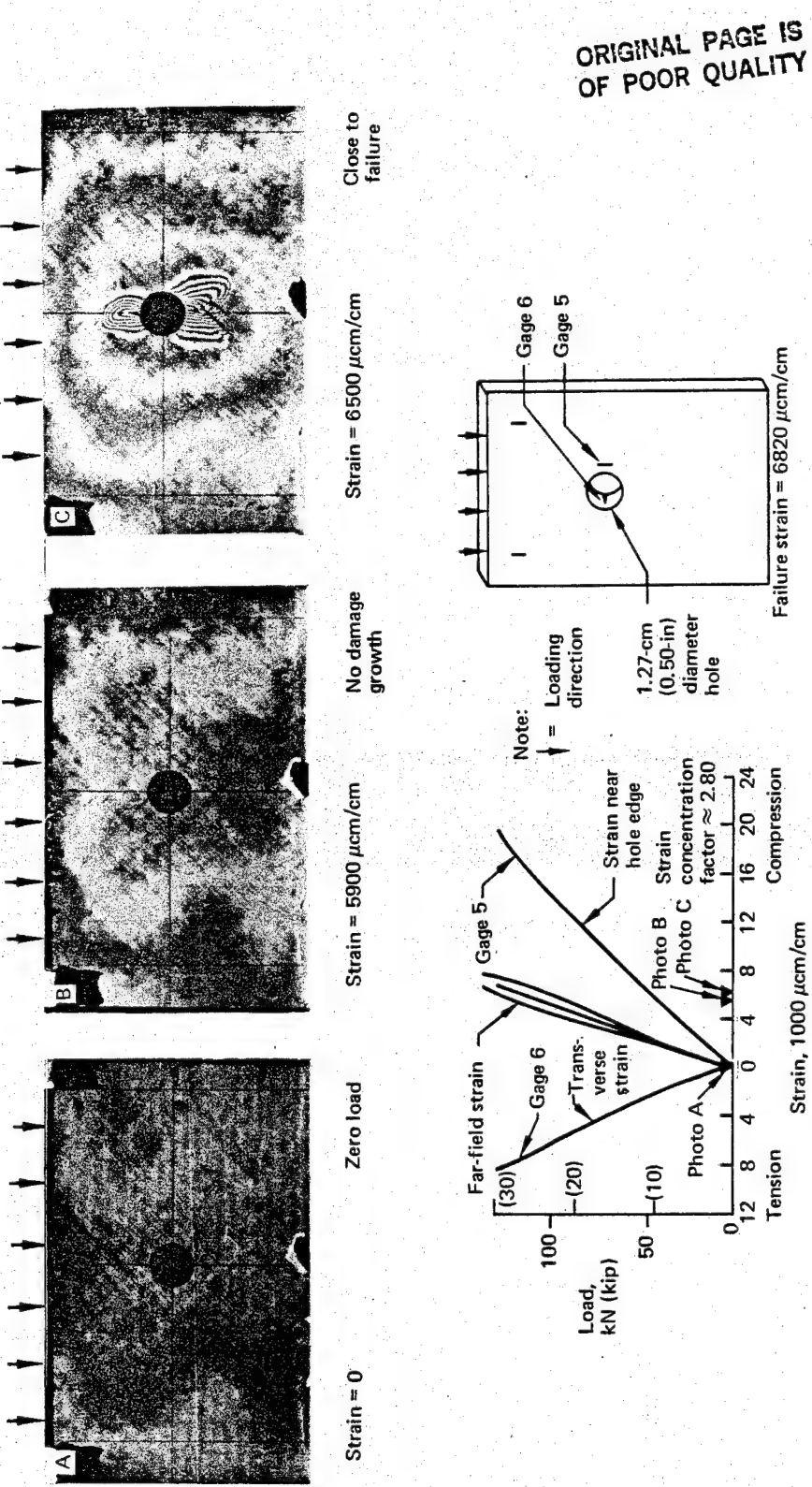


Figure 12. Damage Growth in T300/5208 Circular-Hole Specimen Under Compression Loading

ORIGINAL PAGE IS
OF POOR QUALITY

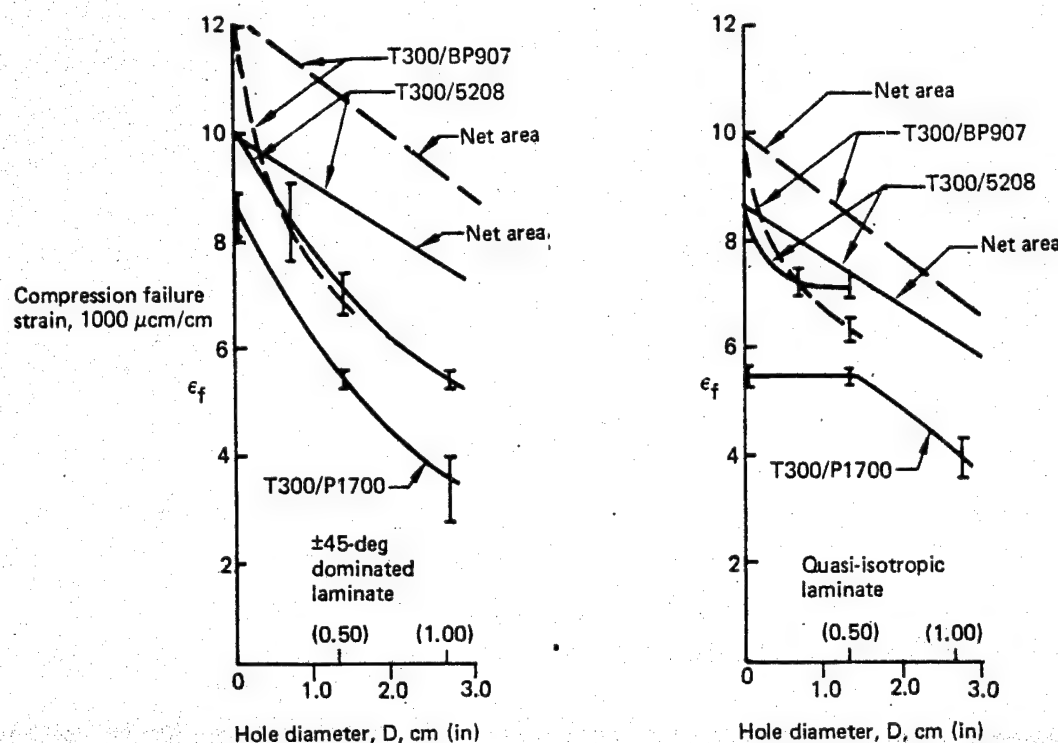


Figure 13. Compressive Failure Strain Decrease With Increasing Hole Diameter

Figure 13 gives a plot of far-field compression failure strain versus hole diameter. To account for the reduction in net area with increasing hole diameter, lines labeled "net area" are superimposed over the experimental data. These net area lines are given by the expression $\epsilon_f = (1 - D/W) \epsilon$, where ϵ_f is the failure strain of a specimen with a hole, ϵ is the failure strain of the specimen with no hole, D is the hole diameter, and W is the specimen width.

Divergence between the experimental failure strain and the net area line with increasing hole diameter demonstrates that strength reduction is not directly related to net area reduction. The polysulfone T300/P1700 results for the nearly quasi-isotropic laminate did not exhibit a large reduction with hole diameter. The low, undamaged, compression failure strain of this laminate makes the T300/P1700 test values questionable. For the two epoxy materials (T300/5208 and T300/BP907), the failure strains for the ± 45 -deg dominated laminates with holes are greater than the nearly quasi-isotropic laminates.

The Figure 14 photographs of failed circular-hole specimens reveal different failure modes. The T300/BP907 and T300/P1700 failures are similar in appearance, with a few planes of delamination on the hole edges. Shear modes and wedging are clearly displayed. T300/5208 exhibits many more planes of delamination than does T300/BP907. As indicated in the test results, failure loads were similar for both epoxy systems (T300/5208 and T300/BP907) in spite of differences in fracture characteristics.

6.3.3 Simulated Delamination Specimens

Specimens with simulated delaminations were evaluated to determine the residual strength and potential delamination growth in the delamination region. Figure 15 provides

**ORIGINAL PAGE IS
OF POOR QUALITY**

Table 7. Circular-Hole Test Results

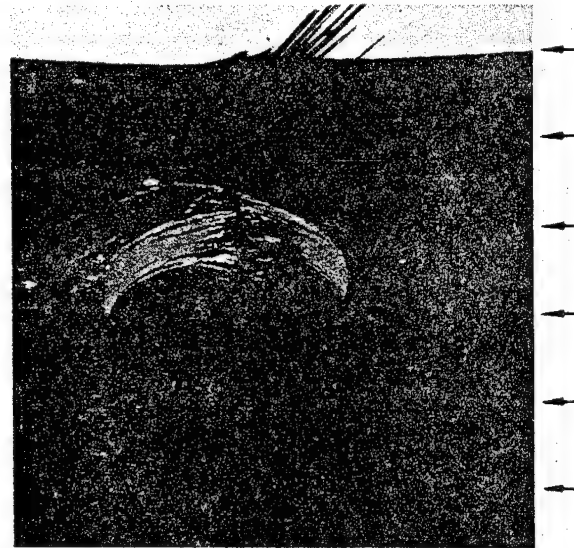
Material	Specimen number	Circular-hole diameter, cm (in)				Failure load, kN (kip)	Failure strain, $\mu\text{cm}/\text{cm}$
		0.64 (0.25)	1.27 (0.50)	2.54 (1.00)	3.81 (1.50)		
T300/5208	11SH1-1	●				173.5 (39.00)	9054
	11SH1-2	●				145.9 (32.80)	7598
	11SH2-1		●			141.0 (31.70)	7143
	11SH2-2		●		●	131.7 (29.60)	6820
	11SH3-1			●		107.6 (24.20)	5304
	11SH3-2			●		106.7 (24.00)	5509
	21SH1-1	●				170.8 (38.40)	7082
	21SH2-2	●				171.3 (38.50)	7164
	21SH2-1		●			171.2 (38.50)	7299
	21SH2-2		●			166.4 (37.40)	6919
T300/BP907	13SH1-1	●				160.1 (36.00)	8069
	13SH1-2	●				163.2 (36.70)	8275
	13SH1-1		●			145.0 (32.60)	7092
	13SH2-2		●			137.0 (30.80)	6691
	13SH3-2			●		111.2 (25.00)	5626
	23SH1-1	●				186.8 (42.00)	7392
	23SH1-2	●				180.1 (40.50)	7118
	23SH2-1		●			160.1 (36.00)	6564
	23SH2-2		●			150.8 (33.90)	6128
T300/P1700	12SH1-1	●				127.0 (28.55)	6428
	12SH1-2	●				119.2 (26.80)	6010
	12SH2-1		●			111.9 (25.15)	5769
	12SH2-2		●			113.0 (25.40)	5828
	12SH3-1			●		92.7 (20.85)	4504
	12SH3-2			●		80.9 (18.20)	3932
	22SH1-1	●				146.8 (33.00)	5571
	22SH2-2	●				95.6 (21.50)	3409
	22SH2-1		●			124.5 (28.00)	5406
	22SH2-2		●			131.7 (29.60)	5719
	12SH3-1			●		60.9 (13.70)	2960
	12SH4-1				●	75.6 (17.00)	3589
	12SH4-2				●	72.1 (16.22)	3424
	12SH4-3				●	59.6 (13.40)	2827
	22SH3-1			●	●	93.2 (20.95)	3697
	22SH3-2			●	●	94.3 (21.20)	3796
	22SH3-3			●	●	96.8 (21.76)	3796
	22SH4-1				●	111.6 (25.10)	4434
	22SH4-2				●	93.8 (21.08)	3752
	22SH4-3				●	96.1 (21.60)	3840

information on the simulated delamination positioning. Inserts were placed between plies of different orientation, where higher interlaminar stresses were expected. The matrix of insert depths consists of 4-, 6-, and 12-ply depths with diameters of 1.27, 2.54, and 3.81 cm (0.5, 1.0, and 1.5 in).

Figure 16 presents some typical experimental results for the insert 3.81 cm (1.5 in) in diameter and four plies deep. The moiré fringe and strain gage record of the laminate surface deformation and resulting delamination growth are shown in the figure.

ORIGINAL PAGE IS
OF POOR QUALITY

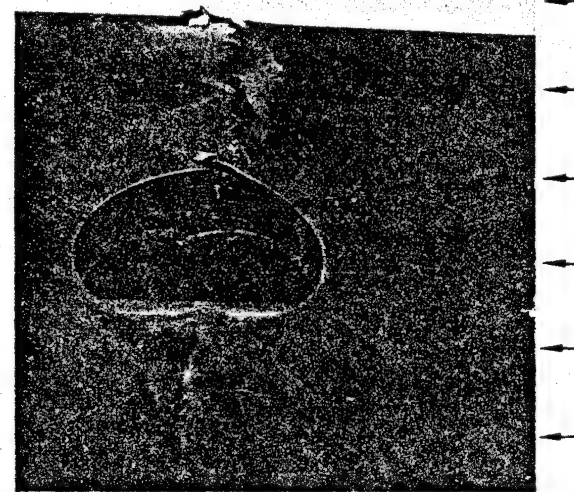
T300/5208
 $\epsilon_{ULT} = 5300 \mu\text{cm}/\text{cm}$



- Failure modes:
 - Delamination
 - Brooming
 - Transverse splitting

Note:
← = Loading
direction

T300/BP907
 $\epsilon_{ULT} = 5630 \mu\text{cm}/\text{cm}$

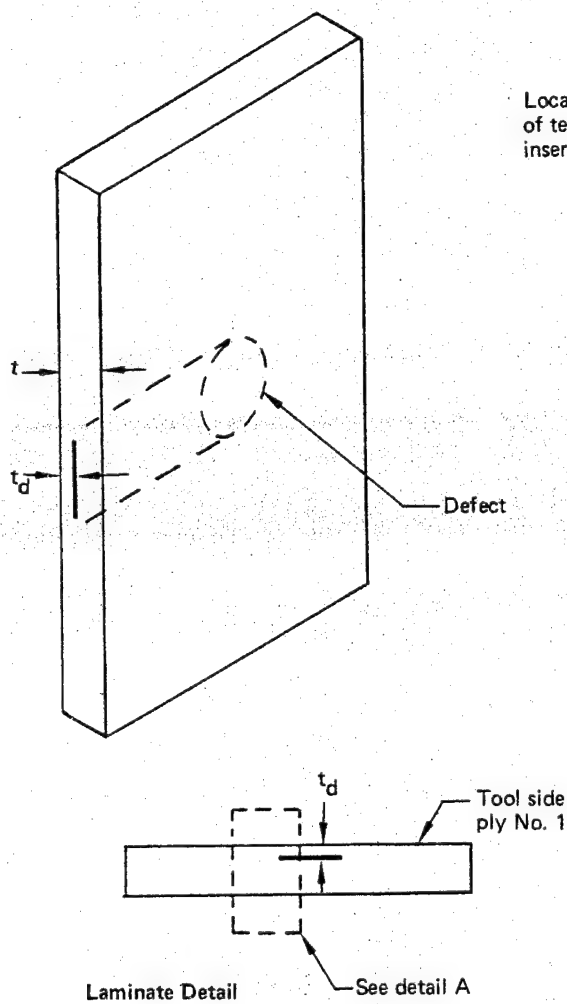


- Failure modes:
 - Some delamination
 - Shear

- ± 45 -deg dominated laminate
- Hole diameter = 2.54 cm (1.0 in)

Figure 14. Failure Mode Comparison of Circular-Hole Specimens

ORIGINAL PAGE IS
OF POOR QUALITY



Detail A

1	+45
2	-45
3	+45
4	-45
5	0
6	0
7	+45
8	-45
9	90
10	+45
11	-45
12	0
13	+45
14	-45
15	90
16	+45
17	-45
18	+45
19	-45
20	+45
21	90
22	-45
23	+45
24	90
25	-45
26	+45
27	0
28	-45
29	+45
30	90
31	-45
32	+45
33	0
34	-45
35	+45
36	-45
37	+45
38	+45

Laminate 2

1	+45
2	-45
3	+45
4	-45
5	0
6	0
7	+45
8	-45
9	90
10	+45
11	-45
12	0
13	+45
14	-45
15	90
16	+45
17	-45
18	+45
19	-45
20	+45
21	90
22	-45
23	+45
24	90
25	-45
26	+45
27	0
28	-45
29	+45
30	90
31	-45
32	+45
33	0
34	-45
35	+45
36	-45
37	+45
38	+45

Laminate 1

Figure 15. Locations of Simulated Delaminations

ORIGINAL PAGE IS
OF POOR QUALITY

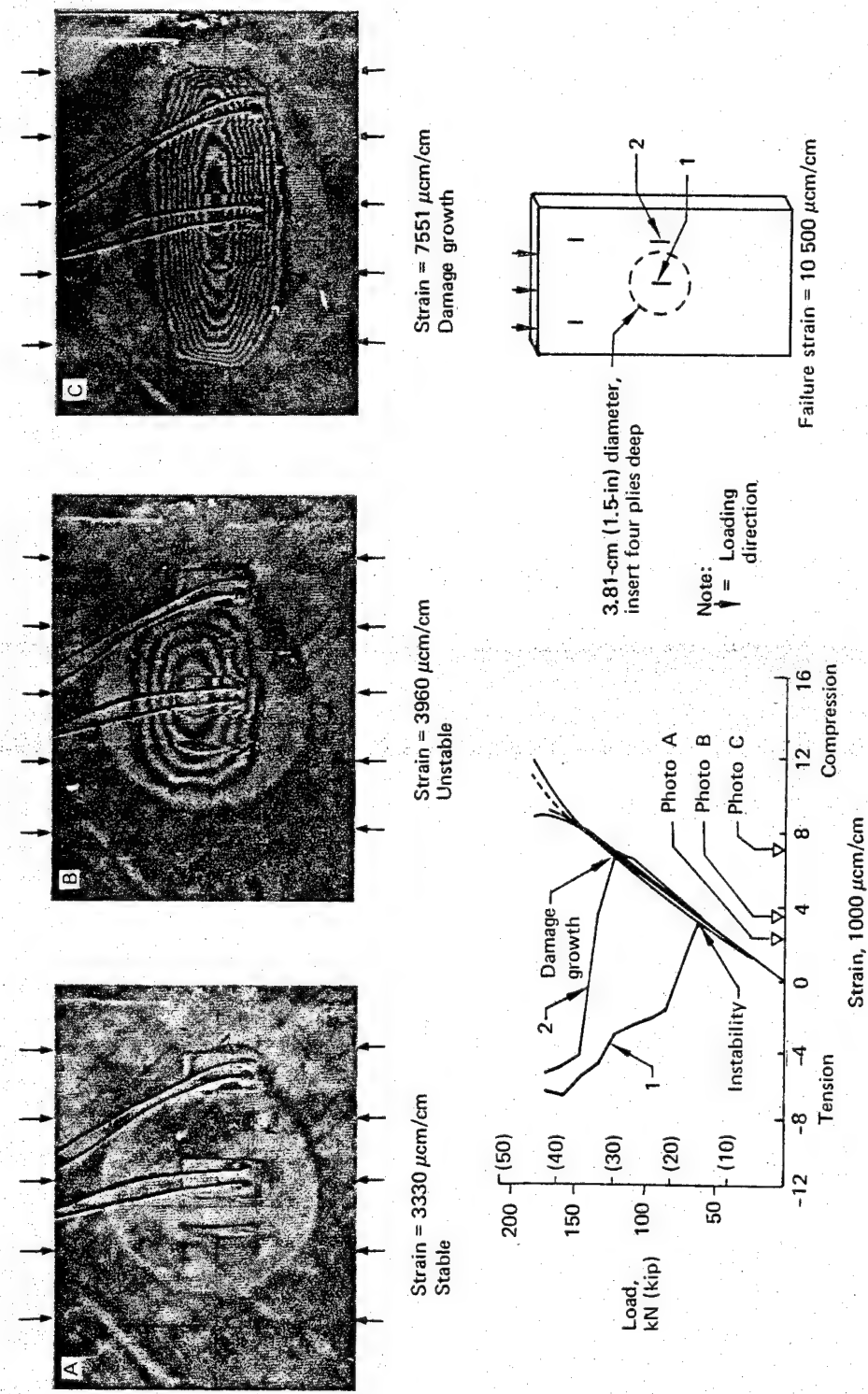


Figure 16. Delamination Growth With Increasing Load—T300/5208

Delamination growth, as determined from experimental observations, is composed of three elements:

1. Instability
2. Initiation and delamination growth
3. Arrest of delamination growth

Some of these characteristics are shown in Figure 16. In photograph A, at a compressive strain of $3330 \mu\text{cm}/\text{cm}$, no instability over the insert has occurred. Increasing the compressive strain results in local instability but no increase in delamination diameter. With still greater compressive strain, delamination growth has initiated, followed by rapid growth and arrest at a new delamination size.

The extent of delamination growth depends on insert diameter and position within the laminate. Delamination growth requires instability. Even with instability, delamination growth may not necessarily occur if the state of stress is below that for growth initiation. Specimen responses may be categorized as follows:

- No instability and no growth
- Instability but no delamination growth initiation
- Instability, initiation, delamination growth, and arrest

From a series of moiré fringe photographs and strain gage data, the correlation between the out-of-plane deformation over the delamination, the delamination width, and the specimen gross strain was determined and is shown in Figure 17.

Some more general experimental observations on delamination growth include the following:

- Delamination growth occurred normal to load direction. In specimens where delaminations grew across the total specimen width, the interaction between the edge supports and the delamination resulted in growth in the loading direction.
- On the specimens where moiré fringe techniques were used, the T300/BP907 material required greater applied strains than T300/5208 to cause delamination growth initiation. This was expected, based on the DCB test results (table 5). In those tests a considerably greater force was required to grow a crack (delamination) in T300/BP907 than in T300/5208.

Table 8 summarizes compression failure strains for the simulated delamination specimens. Test results in the table indicate that delaminations did not result in significant reductions in strength. There are two reasons for this. First, the deepest delaminations did not result in local instability and no growth occurred. Second, large delaminations near the surface became unstable, with resultant extensive delamination of the surface plies; however, the loss of these four low-stiffness surface plies was not significant in relation to remaining plies. Extensive delamination and loss of effective stiffness caused some specimen bending. These test results are pertinent to the laminates, delamination diameters, and depths evaluated in this program.

6.3.4 Impact-Damaged Specimens

Typical experimental results associated with static compression testing of impact-damaged specimens are shown in Figure 18. As in the simulated delamination tests, moiré fringes were used to monitor the growth of delamination in the impact-damaged zone. Out-of-plane deformation in the damage zone occurred at strains as low as $300 \mu\text{cm}/\text{cm}$, as revealed by recorded strain divergence and developed moiré fringe contours in the impacted region.

**ORIGINAL PAGE IS
OF POOR QUALITY**

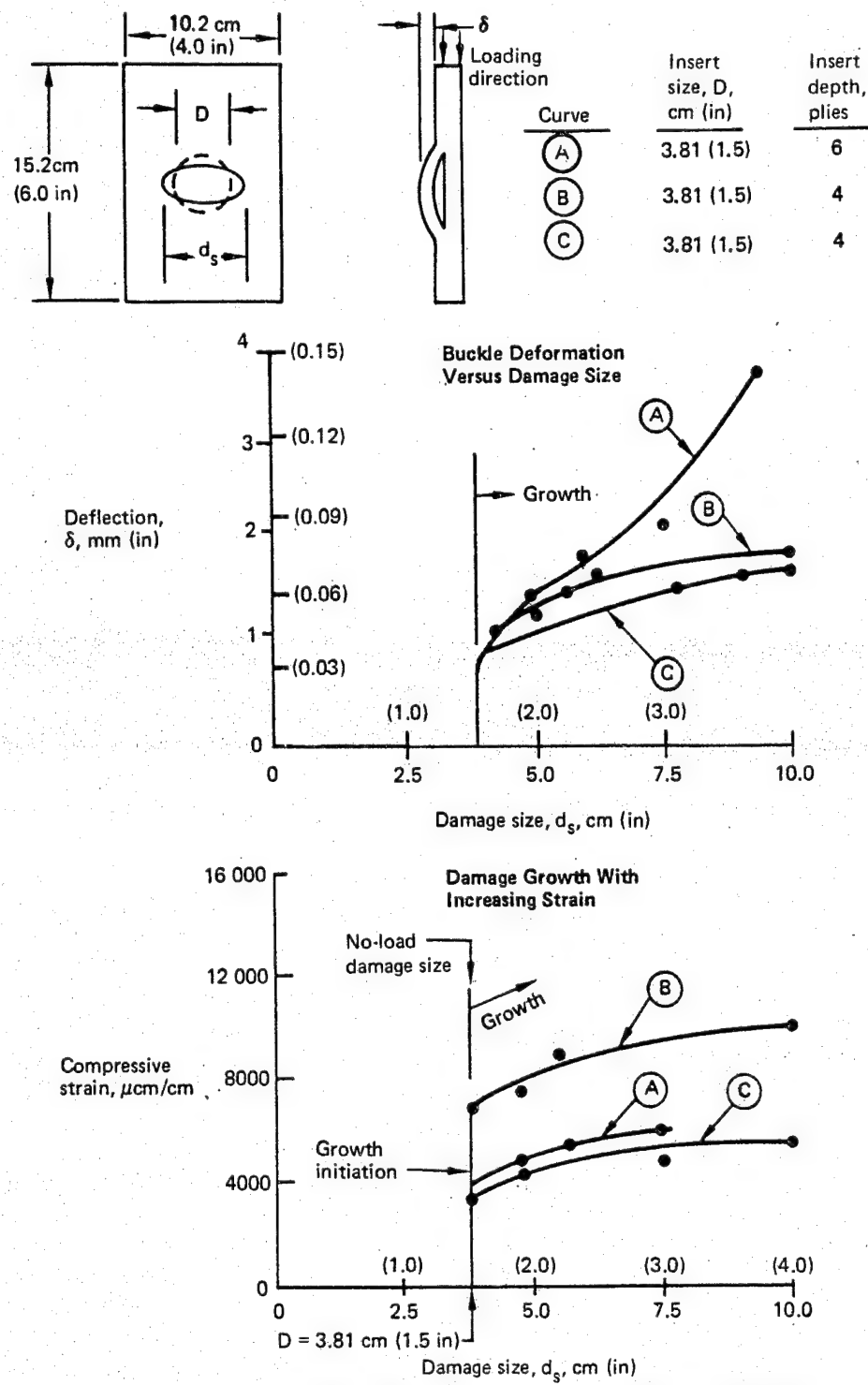


Figure 17. Typical Delamination Growth Characteristics—T300/5208

ORIGINAL PAGE IS
OF POOR QUALITY

Table 8. Simulated Delamination Test Results

Material	Specimen number	Delamination diameter, cm (in)				Delamination depth, plies			Failure load, kN (kip)	Failure strain, $\mu\text{cm}/\text{cm}$
		0.64 (0.25)	1.27 (0.50)	2.54 (1.00)	3.81 (1.50)	4	6	12		
T300/5208	11SD39-1			●		●			190.2 (42.77)	10 141
	11SD39-2			●		●			197.1 (44.30)	10 405
	11SD49-1				●	●			196.7 (44.22)	10 951
	11SD49-2				●	●			164.6 (37.00)	8 564
	21SD29-1				●	●			204.6 (46.00)	8 618
	21SD49-1				●	●			169.9 (37.29)	6 835
	21SD49-2				●	●			173.0 (38.90)	7 132
	11SD26-1		●				●		142.8 (32.10)	7 361
	11SD26-2		●				●		185.9 (41.80)	9 873
	11SD36-1			●			●		171.7 (38.60)	9 050
	11SD46-1				●		●		160.3 (36.04)	8 516
	11SD46-2				●		●		173.4 (39.00)	8 913
	21SD26-1		●				●		239.0 (51.50)	9 596
	21SD26-2		●				●		215.7 (48.50)	9 037
	21SD46-1				●		●		149.4 (33.60)	6 270
	21SD46-2				●		●		146.8 (33.00)	5 993
	11SD23-1		●				●		193.9 (43.60)	10 220
	11SD23-2		●				●		199.3 (44.80)	10 794
	11SD43-1				●		●		180.1 (40.50)	9 490
	11SD43-2				●		●		166.8 (37.50)	8 812
	21SD23-1		●				●		184.1 (41.40)	7 678
	21SD23-2		●				●		207.3 (46.60)	8 539
T300/BP907	13SD39-1			●			●		186.8 (42.00)	9 923
	13SD39-2			●			●		205.5 (46.20)	11 022
	13SD49-1				●		●		219.3 (49.30)	12 171
	13SD49-2				●		●		234.0 (52.60)	9 111
	23SD29-1				●		●		233.9 (52.60)	9 111
	23SD49-1				●		●		226.4 (50.90)	9 285
	23SD49-2				●		●		245.1 (55.10)	10 100
	13SD26-1		●				●		173.5 (39.00)	8 999
	13SD26-2		●				●		183.3 (41.20)	9 546
	13SD36-1			●			●		167.3 (37.60)	8 586
	13SD46-1				●		●		165.9 (37.30)	8 735
	13SD46-2				●		●		163.2 (36.70)	8 584
	23SD26-1		●				●		262.4 (59.00)	10 985
	23SD26-2		●				●		250.0 (56.20)	10 407
	23SD46-1				●		●		213.5 (48.00)	8 650
	23SD46-2				●		●		199.7 (44.90)	8 091
	13SD23-1		●				●		210.4 (47.30)	12 100
	13SD23-2		●				●		174.8 (39.30)	9 100
	13SD43-1				●		●		185.5 (41.70)	9 845
	13SD43-2				●		●		204.2 (45.90)	10 944
	23SD23-1		●				●		249.9 (56.10)	10 469
	23SD23-2		●				●		237.1 (53.30)	9 884

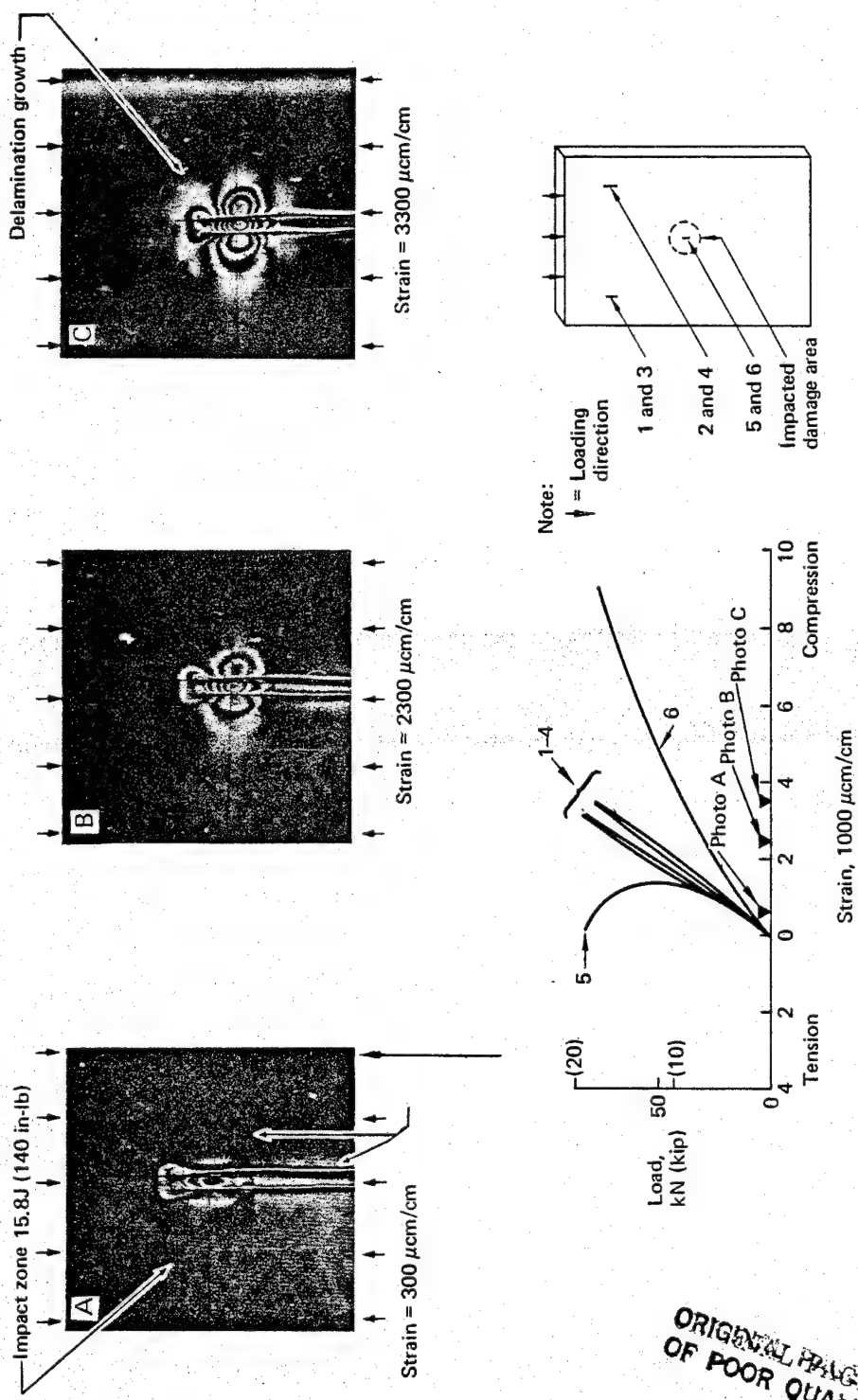


Figure 18. Damage Growth in Impacted T300/5208 Specimens Under Compression Loading

A well-defined elastic instability of surface plies in the impact-damaged region did not occur. This was in direct contrast to the buckling phenomenon associated with simulated delamination specimens. Comparing the strain responses in Figures 16 and 18 shows this difference. Strain divergence in the impact-damaged specimen developed on the initial application of load, whereas no strain divergence occurred in the simulated delamination until the region over the delamination buckled. Delamination growth extended over a small fraction of the specimen width. Specimen failure occurred prior to extensive surface ply delamination. Based on the photomicrographs of impact-damaged T300/5208 laminates that revealed extensive delamination (fig. 11), it is postulated that delamination growth occurred not only between surface plies but between plies throughout the laminate thickness. If so, compression failure would be expected to precede extensive surface delamination growth.

Failure load and strain of impact-damaged specimens are shown in Table 9 and Figure 19. The compressive failure strain is plotted versus kinetic energy of the impactor. As shown in Figure 19, the T300/5208 material demonstrated a dramatic reduction in residual compression strength. The T300/BP907 and T300/P1700 materials exhibited less reduction in residual compression strength than T300/5208 at the higher impact levels. In general, for the three materials, the ± 45 -deg dominated laminates exhibited higher compression failure strain than the nearly quasi-isotropic laminates for a given impact energy level. The residual strength of graphite/epoxy laminates with barely visible damage is of primary concern in evaluating the durability of inservice aircraft components. Components with nonvisually detectable damage traditionally are assumed capable of carrying the ultimate design load. Figure 19 indicates that laminates of different resin systems can produce a large spread in compressive strain capability associated with barely visible damage.

The residual compressive strength of impact-damaged specimens is not directly relatable to damage zone size. Figure 10, presented previously, shows typical ultrasonic through-transmission scans versus compressive failure strains. The failure strain does decrease with increasing damage size for a given material system; nevertheless, the residual compressive strength of different resin laminates with the same damage size is not identical. For example, the strength of T300/BP907 impacted at 31.6J (280 in-lb) was significantly greater than the T300/5208 system impacted at 6.8J (60 in-lb), although damage size appears similar. The photomicrographs of Figure 11 reveal that internal impact-induced fracture damage throughout the laminate thickness in T300/5208 appears more extensive than impact-induced damage in T300/BP907. Based on this comparison, the improved residual compression strength of the T300/BP907 system is not surprising.

6.3.5 Comparison of Results

Differences in Load Versus Strain Response—A number of strain gages were used on some representative specimens of each damage type. Figure 20 presents some typical load strain response data for the T300/5208 tests. Strain gages are shown placed in the specimen corners and in the damaged region (hole, impact, and insert). A comparison of differences in load versus strain response follows:

Comparing the strain response of impact-damaged laminates and laminates with inserts placed on single planes reveals some differences. Gages on the specimen surface near the insert (gages 5 and 6) recorded the strain at which the region over the insert became unstable and the strain at which the effective insert size began to increase. In contrast, surface strain gages on the impact-damaged specimen indicated that out-of-plane bending initiated as soon as load was applied, and no elastic buckling on the surface occurred.

**ORIGINAL PAGE IS
OF POOR QUALITY**

Table 9. Impact-Damaged Specimen Test Results

Material	Specimen number	Impact level, J (in-lb)	Failure load, kN (kip)	Failure strain, $\mu\text{cm}/\text{cm}$
T300/5208	11SI-1	15.8 (140)	86.73 (19.50)	4284
	11SI-2	15.8 (140)	79.62 (17.90)	4094
	11SI-3	11.3 (100)	97.86 (22.00)	4941
	11SI-4	11.3 (100)	89.40 (20.10)	4617
	11SI-5	6.8 (60)	115.70 (26.00)	6023
	11SI-6	6.8 (60)	111.20 (25.00)	5782
	21SI-1	15.8 (140)	85.41 (19.20)	3400
	22SI-2	15.8 (140)	79.62 (17.90)	3290
	22SI-3	11.3 (100)	100.10 (22.50)	4089
	21SI-4	11.3 (100)	90.00 (20.20)	3730
	21SI-5	6.8 (60)	200.20 (45.00)	8400
	21SI-6	6.8 (60)	203.30 (45.70)	8603
T300/BP907	13SI-1	15.8 (140)	213.50 (48.00)	12 277
	13SI-2	15.8 (140)	188.60 (42.40)	10 362
	13SI-3	11.3 (100)	198.70 (44.90)	11 302
	13SI-4	24.9 (220)	164.60 (37.00)	8 580
	13SI-5	31.6 (280)	156.60 (35.20)	7 890
	13SI-6	31.6 (280)	150.80 (33.90)	7 750
	23SI-1	15.8 (140)	240.60 (54.10)	10 169
	23SI-2	15.8 (140)	227.70 (51.20)	9 568
	23SI-3	11.3 (100)	240.20 (54.00)	9 816
	23SI-4	24.9 (220)	161.00 (36.20)	16 500
	23SI-5	31.6 (280)	186.80 (42.00)	7 619
	23SI-6	31.6 (280)	171.20 (38.50)	16 900
T300/P1700	12SI-1	27.1 (240)	117.20 (26.35)	5738
	12SI-2	27.1 (240)	110.80 (24.90)	5416
	12SI-3	19.8 (140)	131.70 (29.50)	6971
	12SI-4	15.8 (140)	127.70 (28.70)	6777
	12SI-5	6.8 (60)	155.70 (35.00)	8061
	12SI-6	6.8 (60)	157.90 (35.50)	8185
	12SI-7	6.8 (60)	132.60 (29.80)	6534
	12SI-8	11.3 (100)	120.10 (27.00)	6148
	12SI-9	11.3 (100)	119.20 (26.80)	6101
	12SI-10	11.3 (100)	141.00 (31.70)	7237
	12SI-11	15.8 (140)	125.40 (28.20)	6426
	12SI-12	21.9 (190)	112.10 (25.20)	5556
	12SI-13	21.5 (190)	123.20 (27.70)	6115
	12SI-14	21.9 (190)	109.00 (24.50)	5399
	12SI-15	11.3 (100)	138.80 (31.20)	5180
	22SI-1	27.1 (240)	120.10 (27.00)	4380
	22SI-2	27.1 (240)	119.60 (26.90)	4367
	22SI-3	15.8 (140)	154.60 (34.75)	5961
	22SI-4	15.8 (140)	137.90 (31.00)	5306
	22SI-5	6.8 (60)	151.50 (34.05)	5718
	22SI-6	6.8 (60)	117.40 (26.40)	4400
	22SI-7	21.5 (190)	110.50 (24.85)	4101
	22SI-8	21.5 (190)	128.10 (28.80)	4772
	22SI-9	31.6 (280)	120.10 (27.00)	4531
	22SI-10	31.6 (280)	117.40 (26.40)	4430

ORIGINAL PAGE IS
OF POOR QUALITY

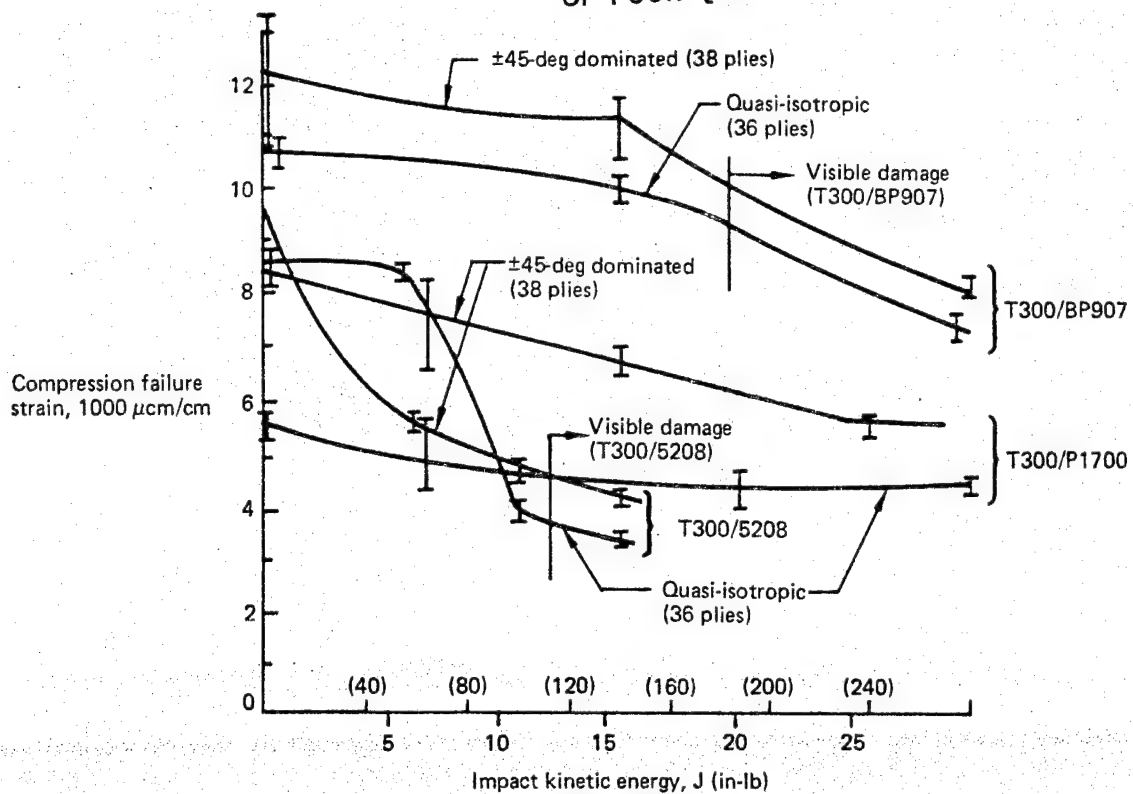


Figure 19. Compressive Failure Strain Reduction With Increasing Impact Energy Levels

Visual and Nondestructive Inspection (NDI) Damage Results—Visual inspectability in metals often provides a basis for evaluating component residual strength. In tension-loaded metal structures the primary mode of fracture is characterized by a growing crack. If crack length can be determined (often only visual inspection is required), the residual strength can be estimated. Conversely, as Figure 21 indicates, the moiré fringe enhanced surface appearance of the damaged graphite/epoxy laminates provides little insight to residual strength of the laminate. The most significant damage results from low-velocity impact, which may shatter the laminate internally but provide little or no visible surface damage. This nonvisually detectable damage seriously reduces compression strength. Clearly this is an undesirable feature in some of the graphite material systems.

Nondestructive, ultrasonic, through-transmission inspection of impact-damaged laminates indicates that damage may be present, but its through-the-laminate thickness distribution is unknown. Figure 22 shows NDI scans of two specimens: one with a 3.81-cm (1.5-in) diameter insert, the other resulting from low-velocity impact. Comparing the failure strains of these two specimens indicates that the appearance of the NDI scan provides an inconclusive (or inaccurate) measure of the real damage in the laminate.

Failure Mode Comparison—Distinct failure mode differences are evident with the different resin systems. Figure 23 is a photograph of failed impact-damaged specimens. The sketches of Figure 24 are drawn from typical failed specimen surfaces and indicate some material failure mode differences. In the T300/5208 material, failures of circular-

ORIGINAL PAGE IS
OF POOR QUALITY

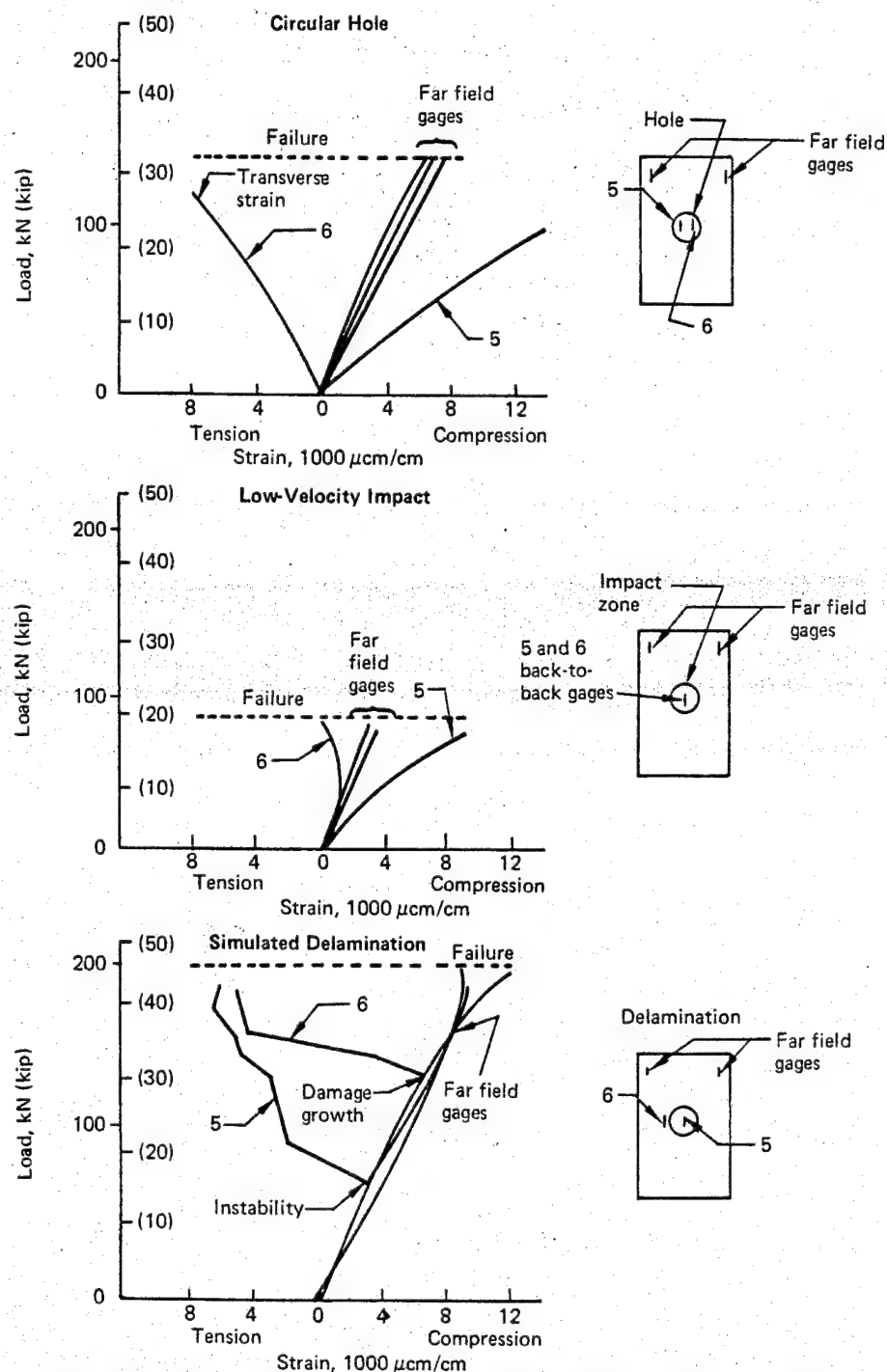


Figure 20. Load Strain Responses of Laminates With Different Types of Damage

ORIGINAL PAGE IS
OF POOR QUALITY

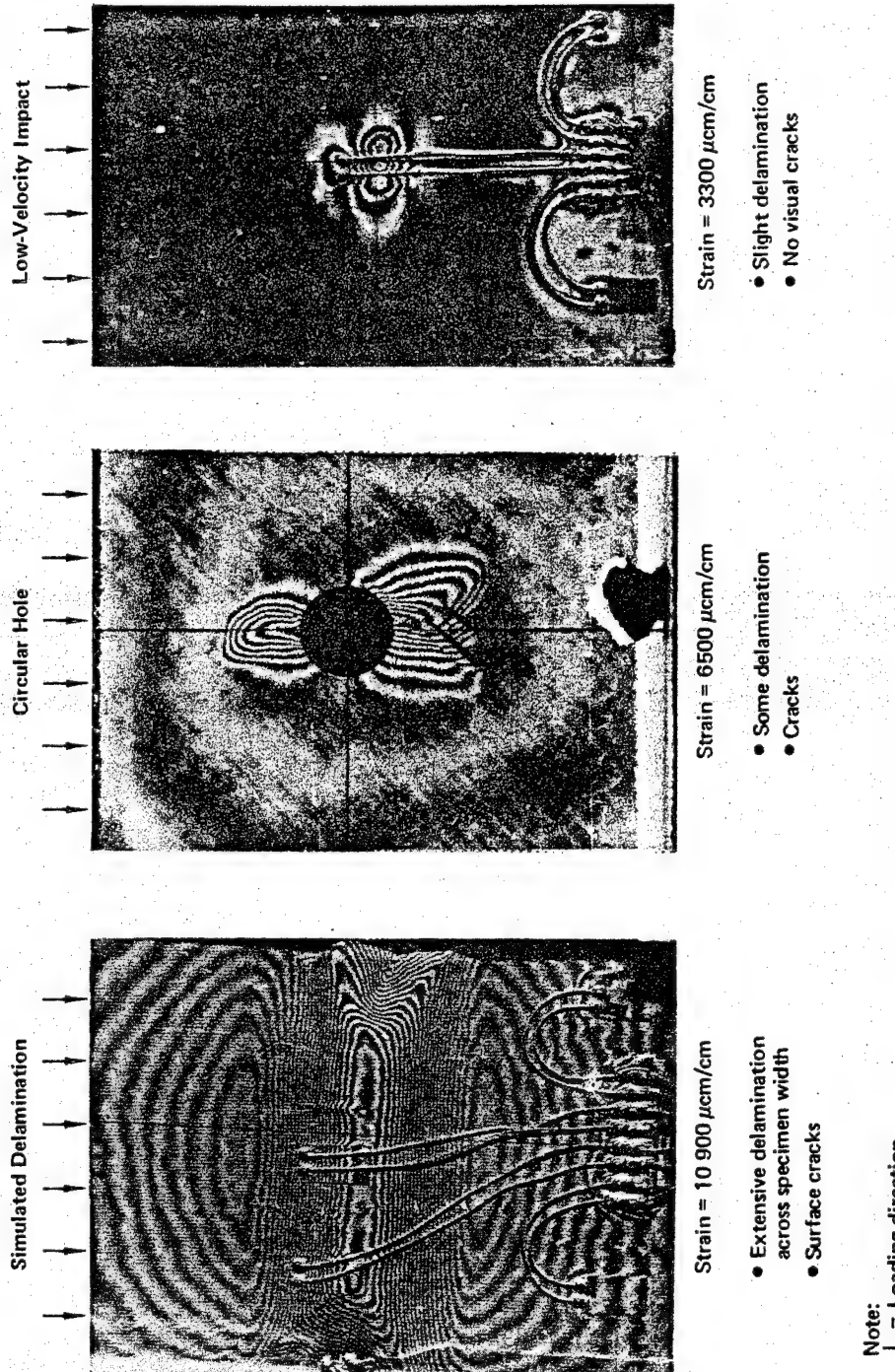


Figure 21. Extent of Surface Damage Prior to Compressive Failure—T300/5208

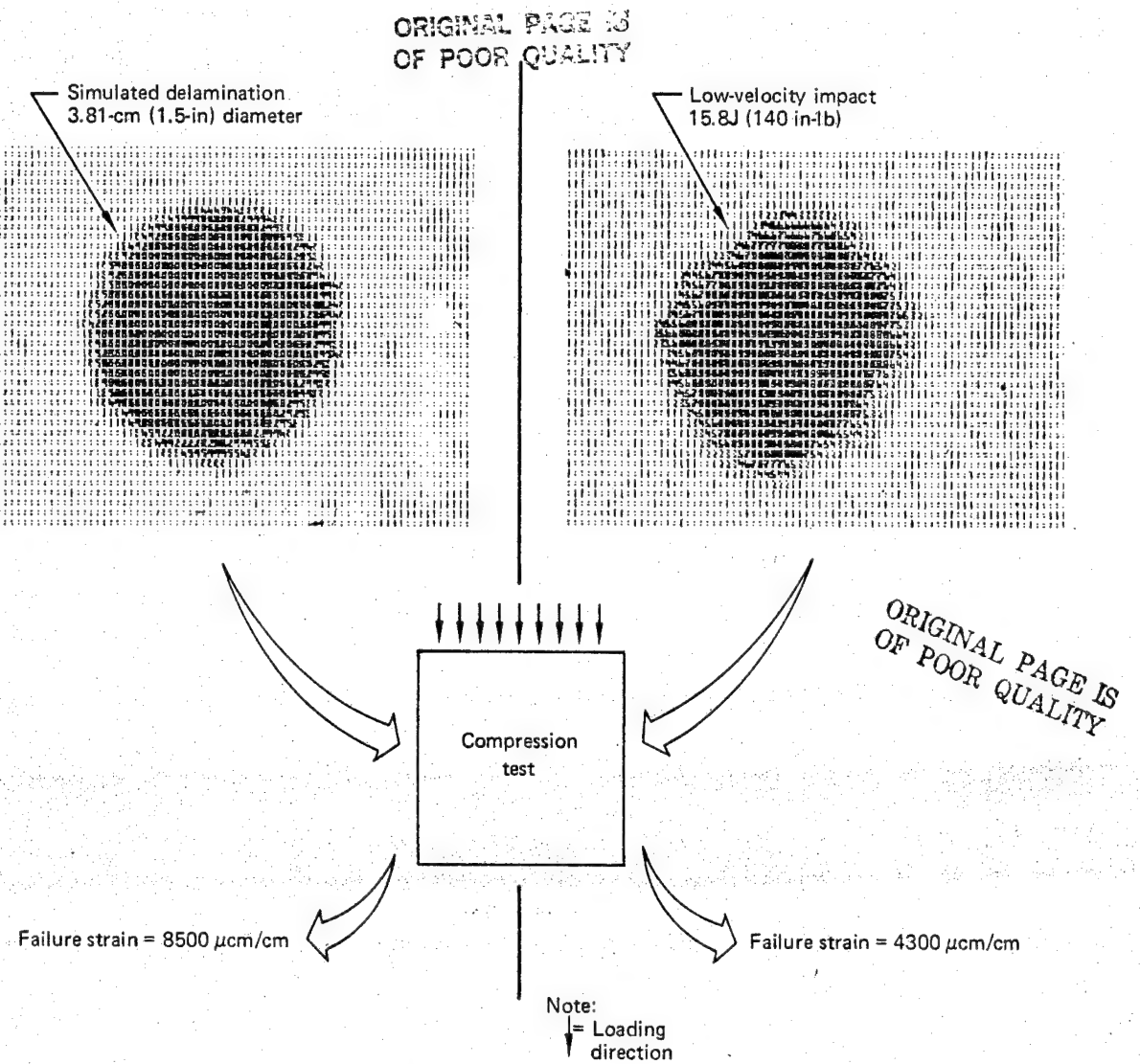
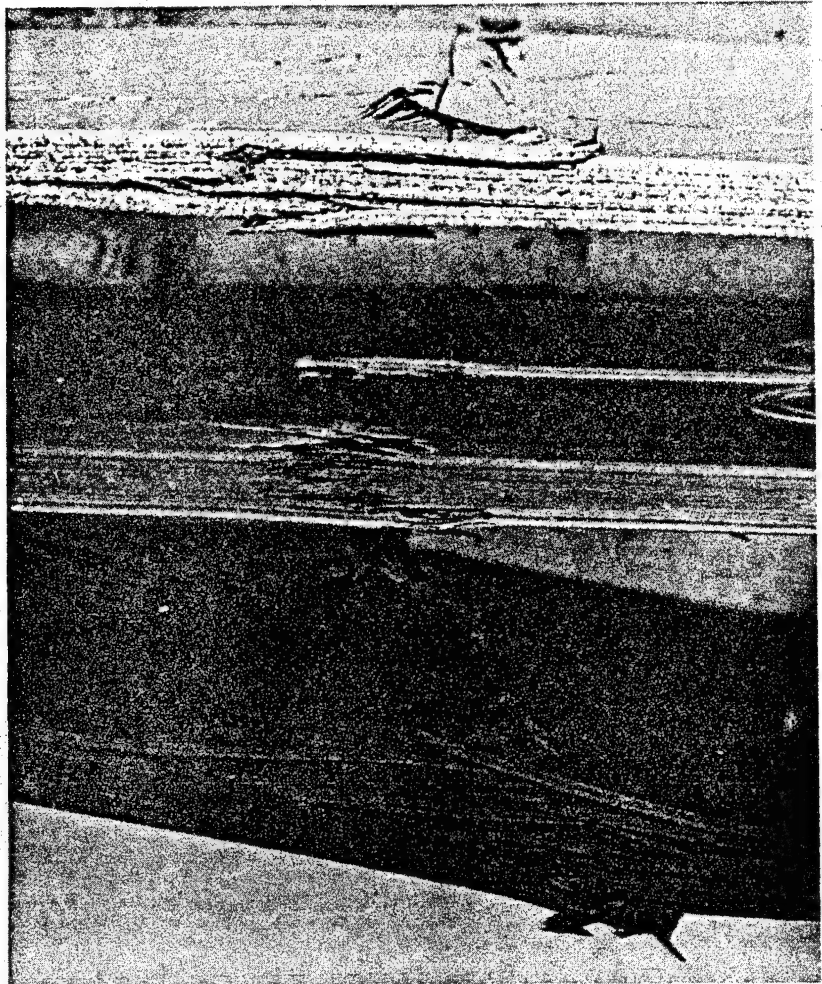


Figure 22. Comparison of Delamination and Impact NDI Scans and Compressive Failure Strain—T300/5208

hole and impact-damaged specimens reveal extensive delamination and "brooming" (fiber splaying). Failed T300/5208 undamaged and simulated delamination specimens typically exhibited a large region of delamination. In the T300/P1700 and T300/BP907 specimens the delamination occurred on fewer planes. Failures in these materials are characterized by shearing modes across the laminate thickness in addition to delamination.

Static Compression Test Summary—Figure 25 summarizes static compression test trends. One of the test objectives was to compare the relative influence of damage type (holes, delamination, and impact) and material systems on residual compression strength. Results given in the figure demonstrate that ranking of damage types changed with the material system. In T300/5208, the impact damage was more severe than circular holes and delamination. In T300/BP907, the severity of damage type changed, with the circular-hole specimens exhibiting the lowest compression strength. Because of the low baseline strength and processing maturity of T300/P1700, the trends shown in the figure should not be considered typical for this material system.



- Impact = 15.8J (140 in-lb)
- ± 45 -deg dominated laminate
- Specimens viewed on edge

T300/P1700
● Shear mode
● Delamination

T300/5208
● Delamination
● Narrow damage zone

T300/BP907
● Shear mode
● Delamination

Figure 23. Failure Mode Comparison of Impact-Damaged Specimens

6.4 CYCLIC COMPRESSION LOADING TESTS

Cyclic compression test apparatus, instrumentation, specimen matrix, and cyclic compression test objectives were discussed previously. This section discusses the experimental observations and compares test results by material, damage type, and cyclic compression strain level.

ORIGINAL PAGE IS
OR POOR QUALITY

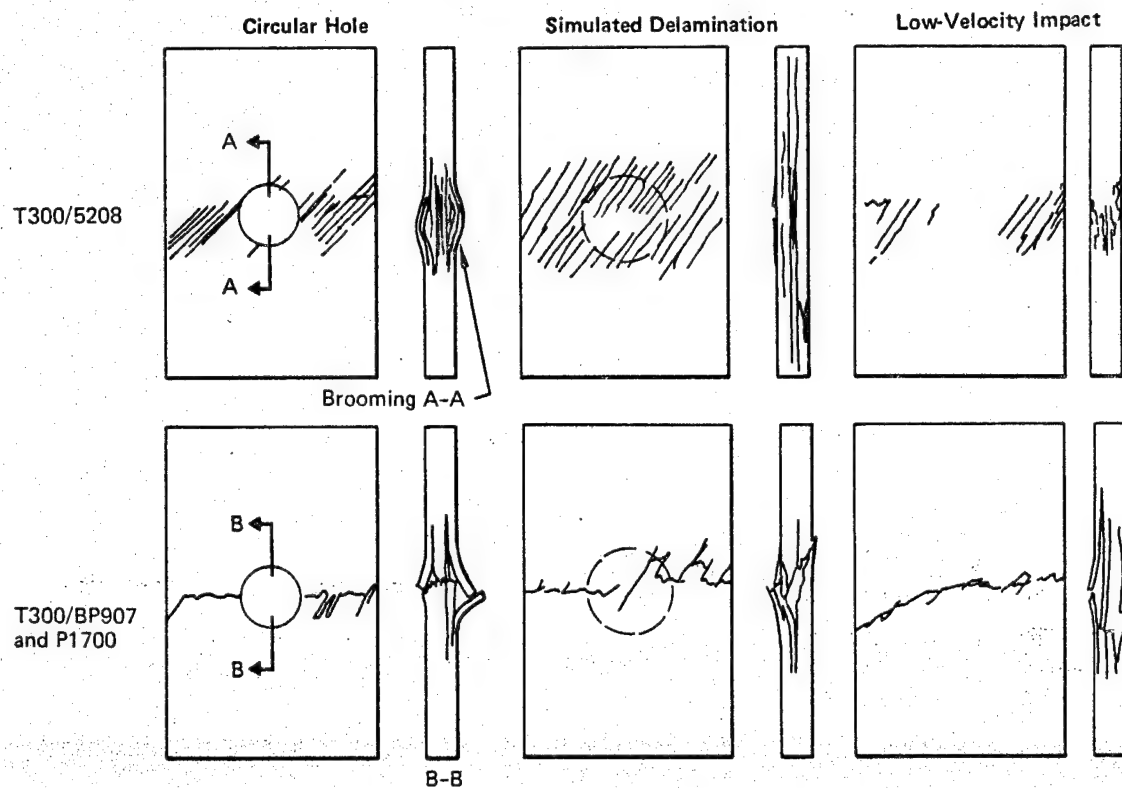


Figure 24. Failure Mode Comparison of Circular-Hole, Simulated Delamination, and Impact-Damaged Specimens

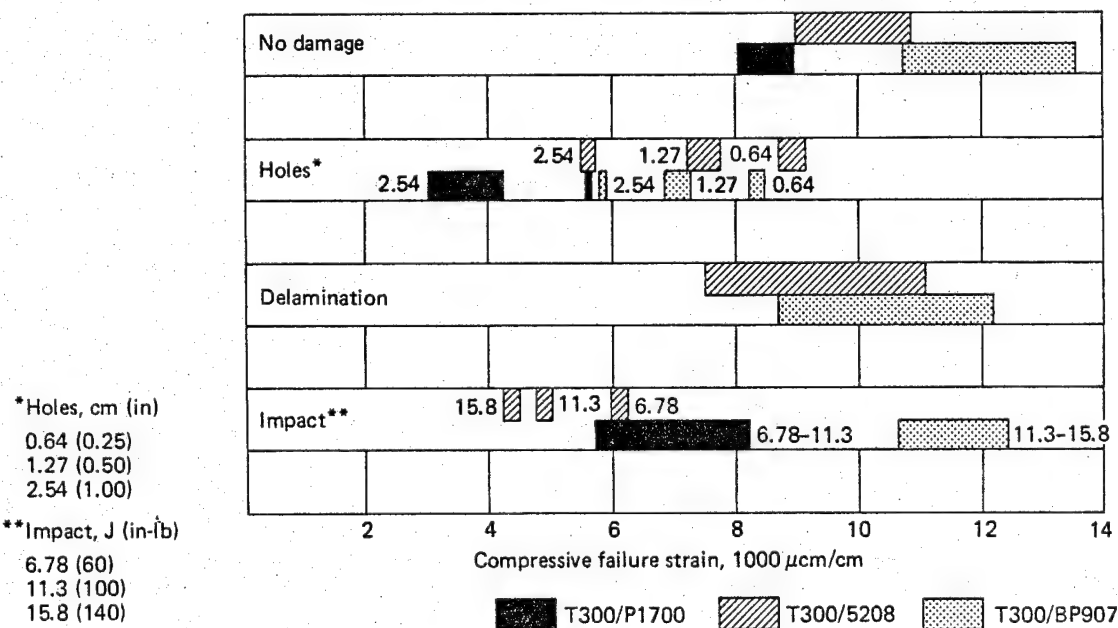


Figure 25. Comparison of Strength, Material, and Damage for $\pm 45\text{-deg}$ Dominated Laminate

**ORIGINAL PAGE IS
OF POOR QUALITY**

6.4.1 Circular-Hole Specimens

Specimens with a hole 1.27 cm (0.50 in) in diameter were selected as baseline specimens for cyclic compression tests in each of the three materials. Some typical experimental results for a T300/5208 laminate with a circular hole are shown in the series of moiré fringe photographs in Figure 26. As indicated, no visible damage was detected following 1 000 980 cycles of cyclic compression strain (in a range of -4000 to -400 $\mu\text{cm}/\text{cm}$) and an additional 5000 cycles of greater cyclic strain (-5000 to -500). With continued cycling at the higher strain level, delamination in the hole region did develop. Associated with the delamination were surface cracks both in the outer ply fiber direction and normal to it. At this strain level, delamination and surface cracking grew rapidly. Specimen failure occurred soon after the appearance of surface damage. The T300/BP907 and T300/P1700 cyclic compression circular-hole specimens did not exhibit delamination. Test results of cyclic compression life versus applied strain level are given in Table 10.

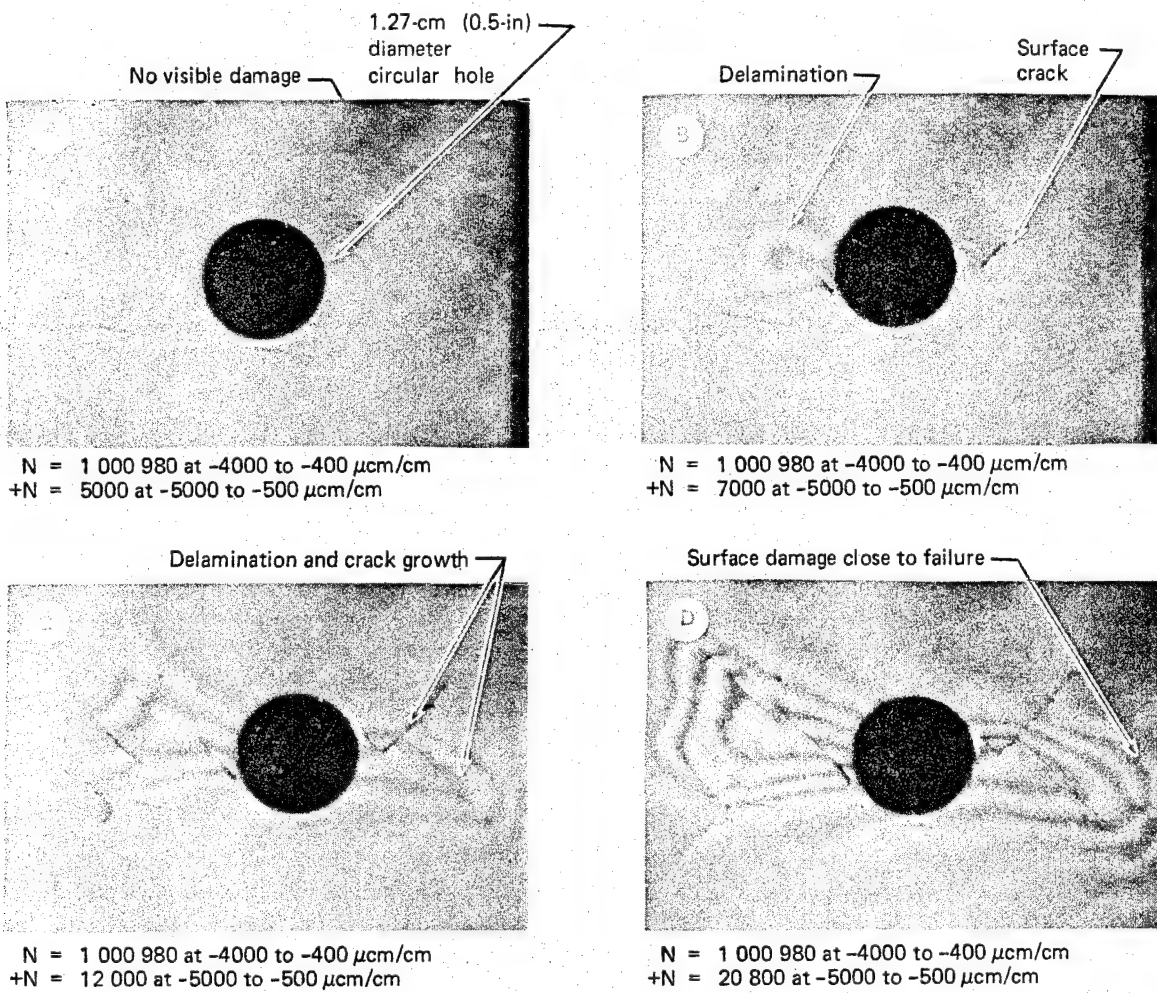


Figure 26. Damage Growth Near a Circular Hole Under Cyclic Compression Loading—T300/5208

Table 10. Cyclic Compression Results for Circular-Hole Specimens

Material	Specimen number	Hole diameter, cm (in)	Cyclic strain range, $\mu\text{cm}/\text{cm}$	Cycles to failure	Comments
T300/5208	11FH2-1	1.27 (0.50)	-4500/-450	1 200 000	
	11FH2-2		-4000/-400	1 000 000	
	11FH2-3		-5000/-500	+19 000	
			-4000/-400	1 000 000	
			-6000/-600	0	Specimen failure at 5780 $\mu\text{cm}/\text{cm}$
	11FH2-4		-4500/-450	750 000	
T300/BP907	11FH2-5		-4000/-400	1 000 000	
	11FH2-6		-5000/-500	+57 000	
			-5000/-500	32 000	
	13FH2-1		-5500/-550	55 000	
	13FH2-2		-5500/-550	54 000	
	13FH2-3		-5000/-500	1 500 000	
T300/P1700	13FH2-4		-5000/-500	300 000	
	13FH2-5		-5500/-550	32 000	
	13FH2-6		-5500/-550	140 000	
	12FH2-2		-5000/-500	3 700	
	12FH2-3		-4500/-450	12 700	
T300/P1700	12FH2-4		-4000/-400	119 000	
	12FH2-5		-3700/-370	256 000	

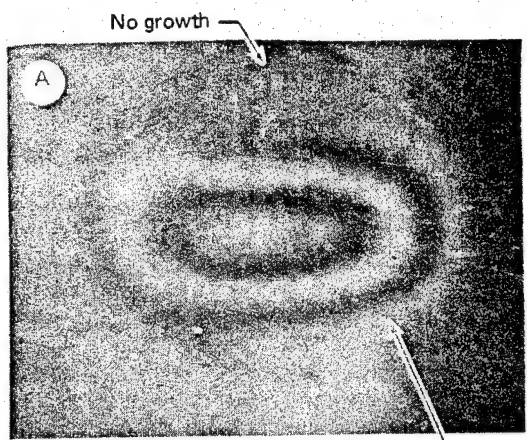
6.4.2 Simulated Delamination Specimens

Some typical results from a sequence of photographs are shown in Figure 27 for T300/5208 and in Figure 28 for T300/BP907.

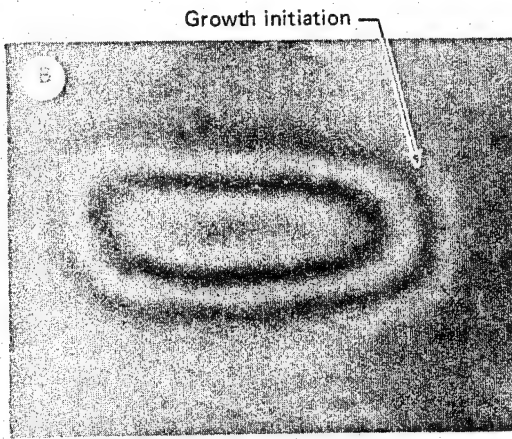
Figure 27 demonstrates delamination growth in T300/5208 under steady cyclic compression loading. The specimen contains a 3.81-cm (1.5-in) diameter insert four plies deep. As shown, no growth occurs up to 955 000 cycles at cyclic strains of -4000 to -400 $\mu\text{cm}/\text{cm}$. As indicated in photograph A, a slight buckle in the delamination region is occurring. Increasing the cyclic strain level to a range of -6000 to -600 $\mu\text{cm}/\text{cm}$ results in growth initiation and propagation. Surface delamination develops across the specimen width prior to failure.

During an attempt to monitor delamination growth in a T300/BP907 specimen with the same simulated delamination size and position, an interesting feature developed. Figure 28 is a series of moire' fringe photographs for this specimen. At the cyclic compression strain level of -6500 to -650 $\mu\text{cm}/\text{cm}$, the region over the delamination buckles on every cycle; however, with an increasing number of cycles, delamination growth initiates in a region away from the specimen edges and initial delamination position. NDI scans prior to testing gave no indication of damage at this location. This behavior was atypical of the simulated delamination cyclic compression tests. Cyclic compression lives for all the simulated delamination tests are summarized in Table 11.

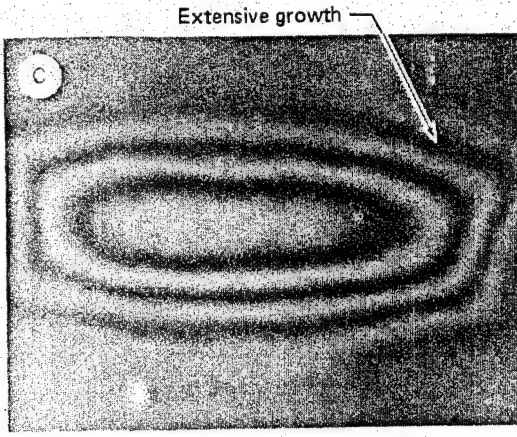
ORIGINAL PAGE IS
OF POOR QUALITY



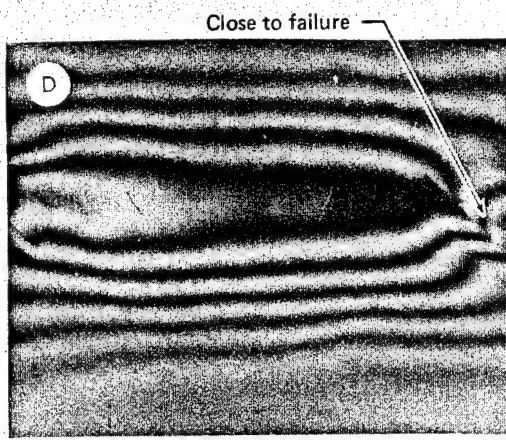
N = 955 000 at -4000 to -400 $\mu\text{cm}/\text{cm}$
Initial defect
3.81-cm (1.5-in)
diameter, 4 plies
deep)



N = 955 000 at -4000 to -400 $\mu\text{cm}/\text{cm}$
+N = 1600 at -6000 to -600 $\mu\text{cm}/\text{cm}$



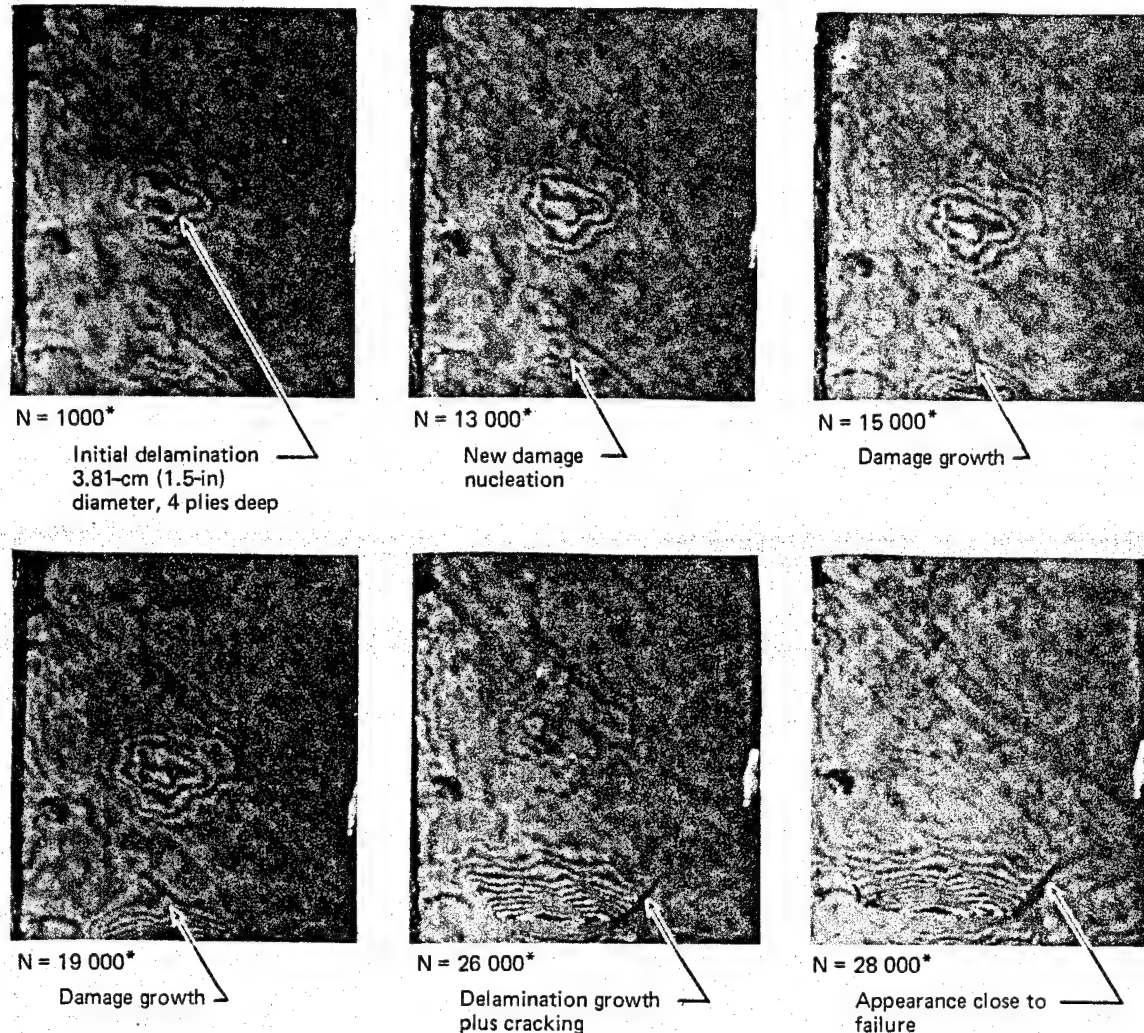
N = 955 000 at -4000 to -400 $\mu\text{cm}/\text{cm}$
+N = 6000 at -6000 to -600 $\mu\text{cm}/\text{cm}$



N = 955 000 at -4000 to -400 $\mu\text{cm}/\text{cm}$
+N = 187 000 at -6000 to -600 $\mu\text{cm}/\text{cm}$

Figure 27. Delamination Growth Under Cyclic Compression Loading—T300/5208

ORIGINAL PAGE IS
OF POOR QUALITY.



*Strain range = -6000 to -600 $\mu\text{cm}/\text{cm}$

Figure 28. Damage Growth in a Simulated Delamination Specimen Under Cyclic Compression Loading—T300/BP907

**ORIGINAL PAGE IS
OF POOR QUALITY**

Table 11. Cyclic Compression Results for Simulated Delamination Specimens

Material	Specimen number	Delamination, cm (in)			Delamination depth, plies			Cyclic strain range, $\mu\text{cm}/\text{cm}$	Cycles to failure	Comments
		1.27 (0.50)	2.54 (1.0)	3.81 (1.50)	4	6	12			
T300/5208	11FD49-1				●	●		-4000/-400 -6000/-600 -8000/-800 -4000/-400 -6000/-600	1 000 000 +1 000 000 +2 200 980 000 660 000	No visible damage
	11FD49-2				●	●		-7000/-700 -4000/-400 -6000/-600	39 000 1 000 000 +240 000	Instability and damage growth
	11FD49-3				●	●		-5600/-650 -6000/-600	84 000 1 100 000	Delamination growth
	11FD49-4				●	●		-7000/-700 -6000/-600	250 000 2 000 000	
	11FD49-5				●	●		-6000/-600	—	
	11FD49-6				●	●		-7666 -8000/-800 -6500/-650	— 88 000 350 000	Static failure near specimen end
	11FD23-1	●					●	-6500/-650	98 000	
	11FD23-2	●					●	-8000/-800 -8000/-800	7 200 33 000	
	11FD23-3	●					●	-6500/-650	410 000	
	11FD23-4	●					●	-7000/-700	290 000	
	11FD23-5	●					●	-6000/-600	1 700 000	
	11FD23-6	●					●	-4000/-400 -6000/-600	1 000 000 +1 000 000	
	11FD43-1						●	-8000/-800	+6 600	
	11FD43-2						●			
	11FD43-3						●			
T300/BP907	13FD49-1				●	●		-8000/-800	33 000	
	13FD39-2				●	●		-7000/-700	120 000	
	13FD49-3				●	●		-6500/-650	140 000	
	13FD49-4				●	●		-7000/-700	50 000	
	13FD49-5				●	●		-7500/-750	14 000	
	13FD49-6				●	●		-6000/-600	790 000	
	13FD23-1	●					●	-6500/-650	35 000	
	13FD23-2	●					●	-6500/-650	110 000	
	13FD23-3	●					●	-7000/-700	7 900	
	13FD23-4	●					●	-8000/-800	11 000	
	13FD23-5	●					●	-7000/-700	1 500 000	
	13FD23-6	●					●	-7000/-700	370 000	
	13FD43-1				●		●	-7000/-700	530 000	
	13FD43-2				●		●	-7500/-750	23 000	
	13FD43-3				●		●	-7500/-750	160 000	
	13FD43-4				●		●	-8000/-800	8 800	Failure near specimen end
	13FD43-5				●		●	-7000/-700	16 000	
	13FD43-6				●		●	-7000/-700	67 000	

6.4.3 Impact-Damaged Specimens

In contrast to the simulated delamination specimens, delamination growth under cyclic compression loading of impact-damaged specimens was not as extensive. In Figure 29, one typical moire fringe photograph sequence for a T300/5208 specimen shows early delamination but little growth until catastrophic failure. The test results given in Table 12 indicate that impact-induced damage may seriously degrade cyclic compression quality. Because of their low strain capability with impact damage, the T300/5208 specimens were cycled at lower compression loads than the T300/P1700 and T300/BP907.

6.4.4 Comparison of Results

Results of the cyclic compression tests are plotted in Figures 30 through Figure 32 by material system. These three curves show how various damage types influence cyclic compression capability. As shown, nonvisually detectable impact damage in T300/5208 results in low static compression strength, as discussed previously, and large reduction in cyclic compression life. T300/BP907 specimens with visually detectable impact damage exhibit greater cyclic compression capability than T300/5208.

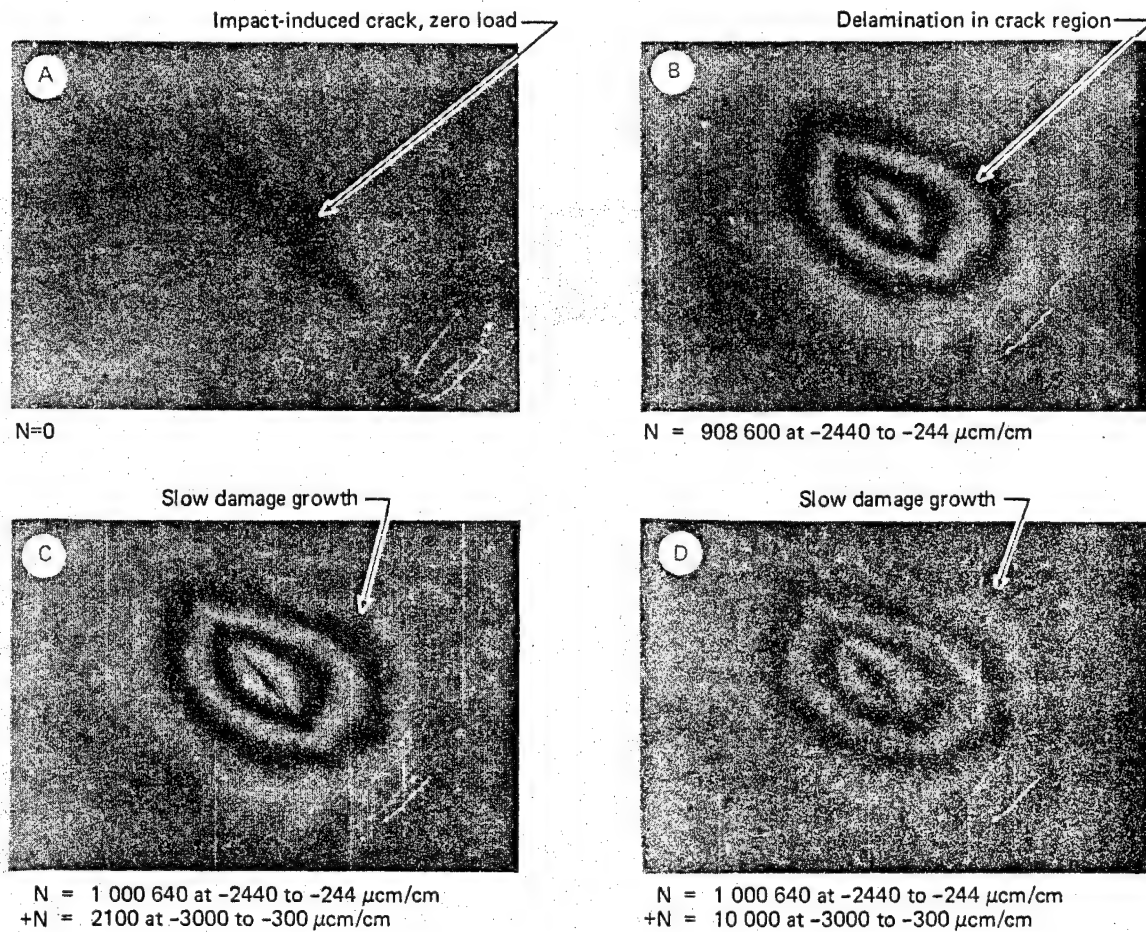


Figure 29. Damage Growth in an Impacted Specimen Under Cyclic Compression Loading-T300/5208

Table 12. Cyclic Compression Results for Impact-Damaged Specimens

Material	Specimen number	Impact energy level, J (in-lb)	Cyclic strain range, $\mu\text{cm}/\text{cm}$	Cycles to failure	Comments
T300/5208	11FI-1	15.8 (140)	-3000/-300 -4000/-400	1 000 000 1 800	
	11FI-2	15.8 (140)	-4000/-400	—	Static failure below -4000 strain
	11FI-4	15.8 (140)	-2440/-244 -3000/-300	1 000 000 +920 000	
	11FI-6	15.8 (140)	-3500/-350	3 300	
	11FI-7	6.78 (60)	-5000/-500	1 700 000	
	11FI-8	6.78 (60)	-4000/-400 -6000/-600	1 000 000 7 500	Failure near specimen end
	11FI-9	6.78 (60)	-4000/-400	1 600 000	
	11FI-10	6.78 (60)	-4000/-400	340 000	
	11FI-11	6.78 (60)	-4500/-450	800 000	
	11FI-12	6.78 (60)	-5000/-500	9 600	
	13FI-1	15.8 (140)	-8000/-800	79 000	
	13FI-2	15.8 (140)	-7000/-700 -7500/-750	1 500 000 +51 000	
T300/BP907	13FI-3	15.8 (140)	-8000/-800	7 400	
	13FI-4	15.8 (140)	-7500/-750	380 000	
	13FI-5	15.8 (140)	-7500/-750	20 000	
	13FI-6	15.8 (140)	-7000/-700	850 000	
	13FI-7	31.6 (280)	-6000/-600	41 000	
	13FI-8	31.6 (280)	-5500/-550	110 000	
	13FI-9	31.6 (280)	-7000/-700	4 300	
	13FI-10	31.6 (280)	-6000/-600	32 000	
	13FI-11	31.6 (280)	-5000/-500 -6000/-600	900 000 26 000	
	13FI-12	31.6 (280)	-5000/-500 -6000/-600	4 000 000 45 000	
	12FI-7	6.78 (60)	-7000/-700	2 340	
	12FI-8	6.78 (60)	-6000/-600	15 300	
T300/P1700	12FI-9	6.78 (60)	-5000/-500	107 830	
	12FI-10	6.78 (60)	-4700/-470	583 550	
	12FD23-1*	15.8 (140)	-5000/-500	5 290	
	12FD23-2*	15.8 (140)	-4500/-450	64 030	
	12FD23-3*	15.8 (140)	-4000/-400	139 300	
	12FD23-4*	15.8 (140)	-3700/-370	333 900	

*An explanation of these specimens is presented in Section 6.3.4

ORIGINAL PAGE IS
OF POOR QUALITY

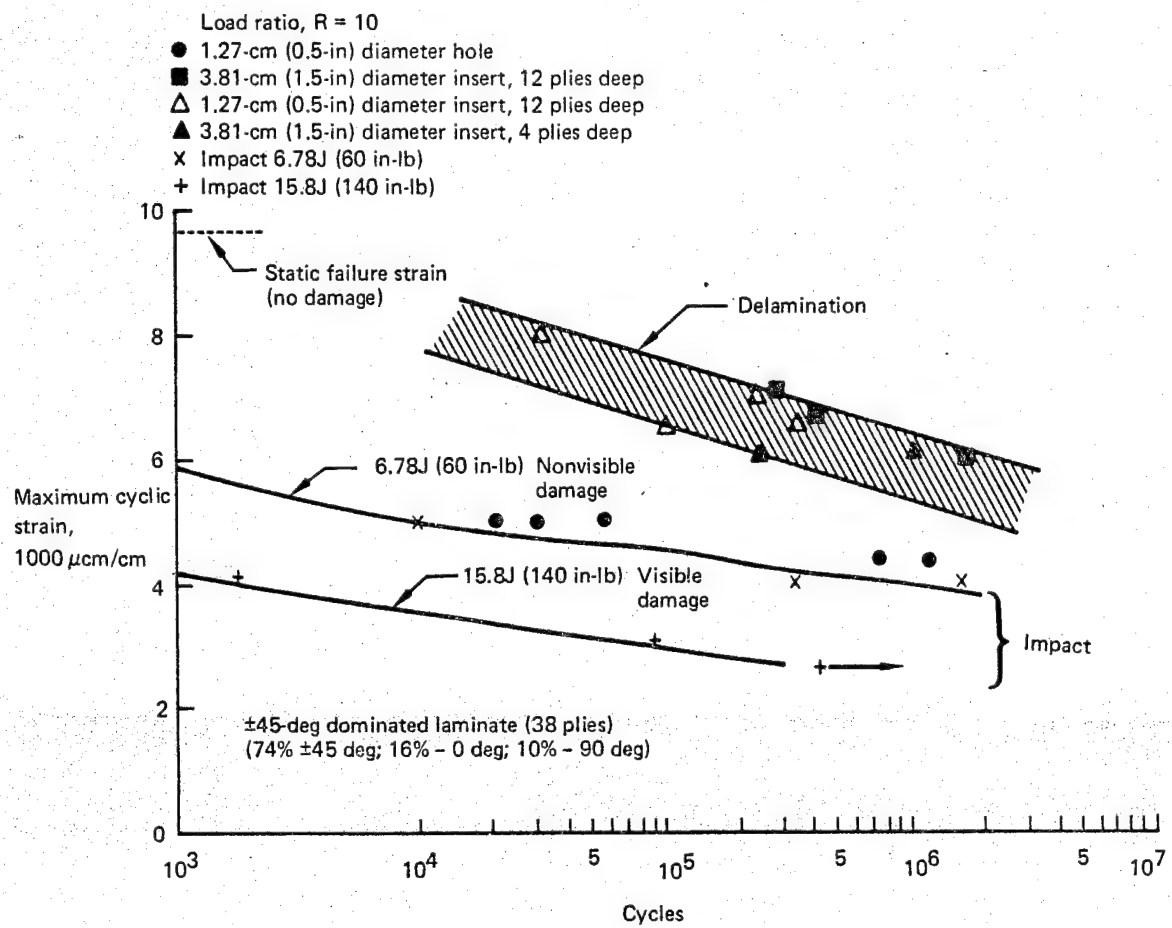


Figure 30. Cyclic Compression Life Trends—T300/5208

No cyclic compression tests of undamaged specimens were evaluated. The specimens with simulated delaminations exhibited high cyclic compression quality, probably comparable to undamaged laminate capability.

The relative effect of circular holes on cyclic compression life changed with the material system. In T300/5208, impact was the most severe damage type; in T300/BP907, holes were more critical. Cyclic compression lives for the different materials and damage types are compared in Table 13.

The table gives order-of-magnitude cyclic compression lives for each material and damage type evaluated. The most dramatic differences are associated with impact damage. For an impact of 15.8J (140 in-lb), cyclic compression lives exceeding 10^6 cycles at cyclic strains of $-7000 \mu\text{cm}/\text{cm}$ are obtained in T300/BP907, but this strain level is above the static failure strain for the other materials. From the test results, the cyclic compression quality of the materials may be ranked by damage type. The T300/BP907 demonstrated higher cyclic compression life for all damage types in comparison to

ORIGINAL PAGE IS
OF POOR QUALITY

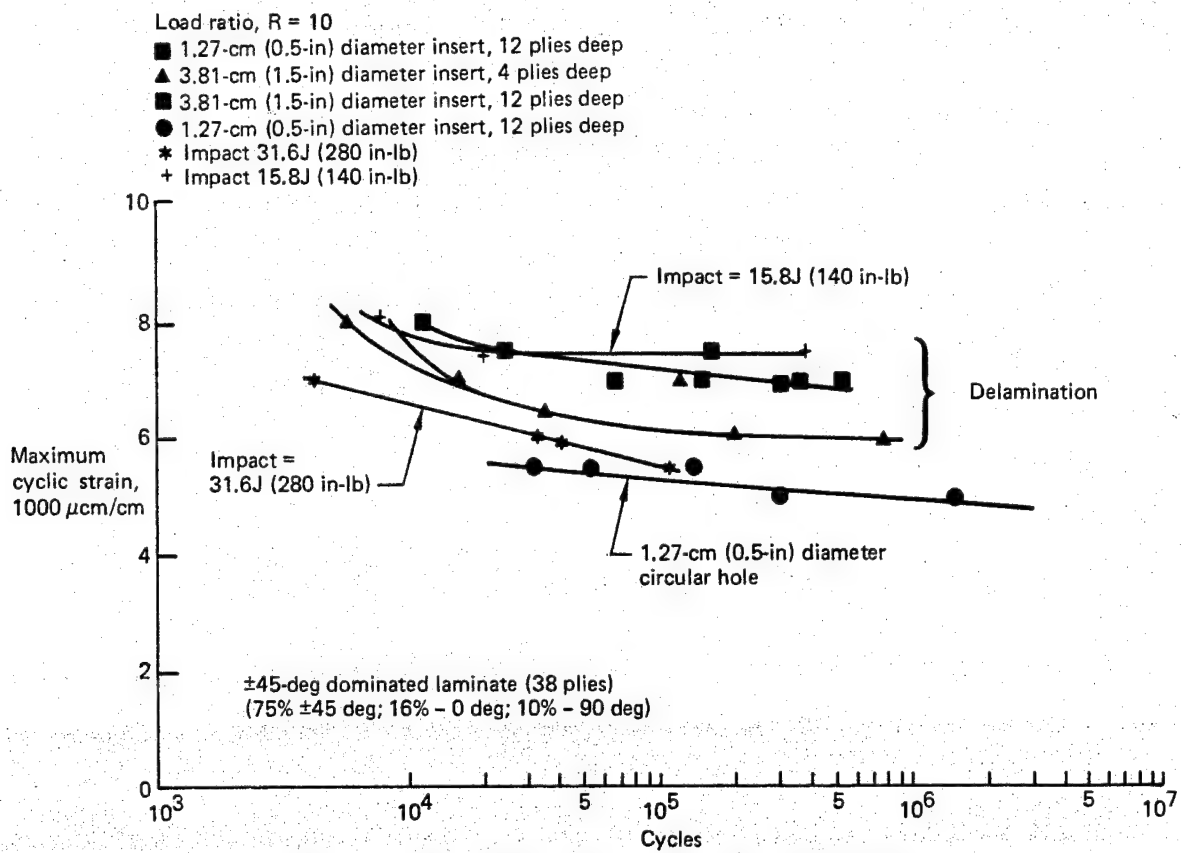


Figure 31. Cyclic Compression Life Trends—T300/BP907

T300/5208. The T300/5208 cyclic compression degradation of laminates with circular holes was less than T300/P1700; however, the T300/5208 degradation associated with impact damage was greater than the T300/P1700.

Failed cyclic compression specimens were inspected visually for comparison with static failure modes, which are described in Table 14. With the exception of some T300/5208 specimens, the cyclic compression failure modes are similar to the static failure modes described earlier. The T300/5208 simulated delamination specimens exhibited extensive delamination on many planes. Delamination extended to loaded edges and specimen ends. In the T300/5208 impact and hole specimens, damage propagated across the specimen width, leaving specimen loading ends intact.

These results are based on the laminates, hole size, delamination parameters, and impact levels evaluated in these tests. Extrapolation of the conclusions drawn here to other material systems or test conditions could be misleading.

ORIGINAL PAGE IS
OF POOR QUALITY

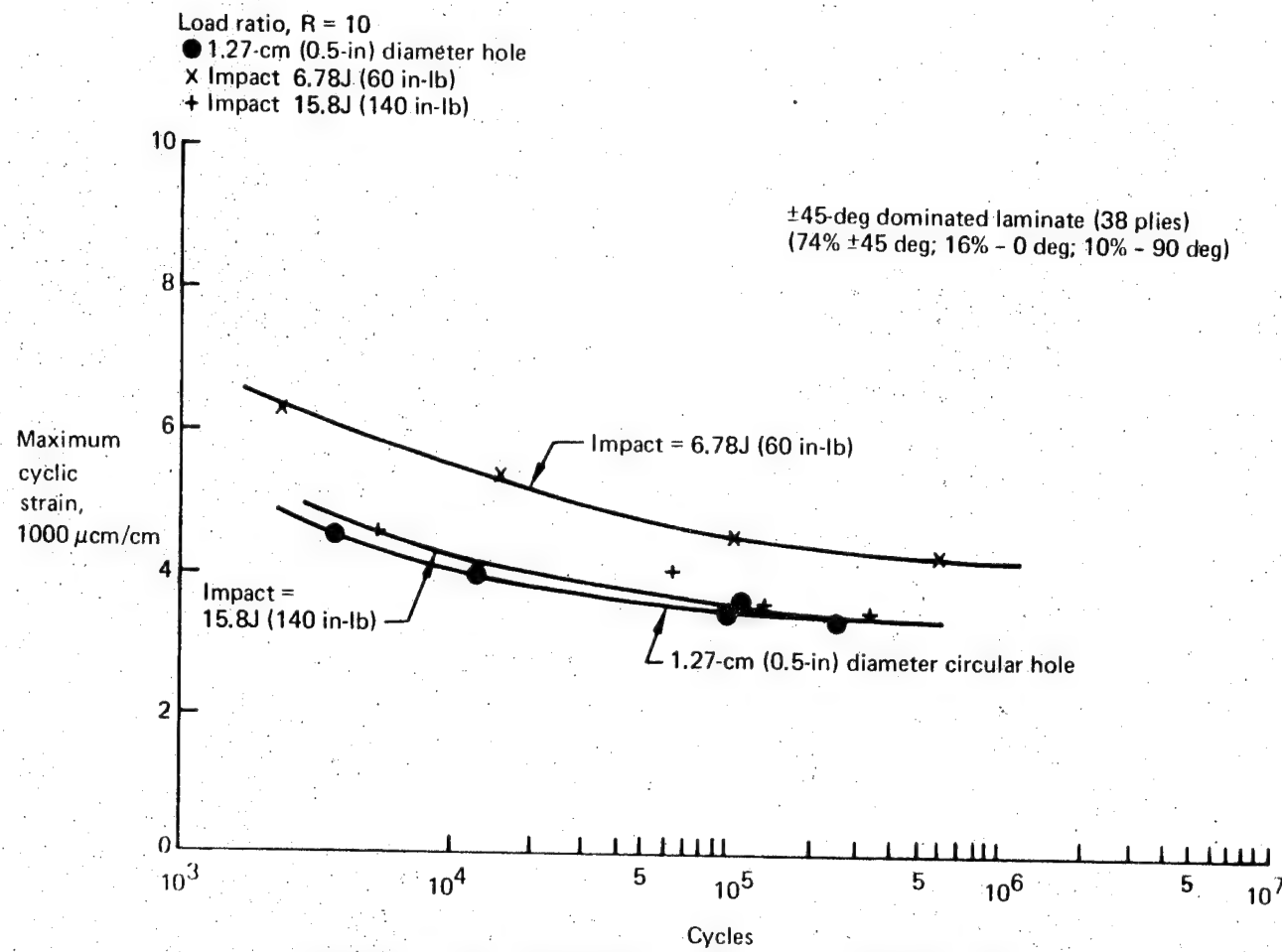


Figure 32. Cyclic Compression Life Trends – T300/P1700

ORIGINAL PAGE IS
OF POOR QUALITY

Table 13. Comparison of Cyclic Compression Lives by Strain Level, Material, and Specimen Type

Maximum compressive strain, $\mu\text{cm}/\text{cm}$	Simulated delamination	Specimen type					
		Impact-damaged			Circular-hole, 1.27-cm (0.50-in) diameter		
		6.8J (60 in-lb)	15.8J (140 in-lb)	31.6J (280 in-lb)	T300/ P1700	T300/ BP907	T300/ P1700
		T300/ 5208	T300/ P1700	T300/ 5208	T300/ P1700	T300/ 5208	T300/ P1700
-4000	No test conducted	$10^5 \cdot 10^6$	No test conducted	10^3	10^5	10^3	No test conducted
-5000	S	S	10^5	S	10^3	$>4 \times 10^6$	$10^4 \cdot 10^6$
-6000	10^6^*	$>2 \times 10^6$			S	10^4	S
-7000	$10^4 \cdot 10^5$	$10^4 \cdot 10^6$			10^6	10^3	S
-8000	$10^3 \cdot 10^4$	$10^3 \cdot 10^4$			10^3		S

S Strain level exceeds static failure strain

> Indicates test was terminated without failure

* Cyclic compression life

ORIGINAL PAGE IS
OF POOR QUALITY

Table 14. Results of Postfailure Analysis

Specimen type	T300/5208	T300/BP907	T300/P1700
Circular holes	<ul style="list-style-type: none">● Extensive delamination planes on hole edge	<ul style="list-style-type: none">● Shear mode● Minor delamination on hole edge● Appearance similar to static failure	<ul style="list-style-type: none">● Similar to BP907
Simulated delamination (inserts)	<ul style="list-style-type: none">● Extensive delamination on many planes over a large portion of specimen● Extensive surface damage; cracks	<ul style="list-style-type: none">● Shearing and wedging in addition to a few major planes of delamination● Appearance similar to static failure	<ul style="list-style-type: none">● No test conducted
Low-velocity impact	<ul style="list-style-type: none">● Shearing and brooming on specimen edges● Damaged strip across specimen width	<ul style="list-style-type: none">● Shearing and a few long planes of delamination (appearance similar to delamination specimens)● Appearance similar to static failure	<ul style="list-style-type: none">● Similar to BP907

7.0 CONCLUSIONS

Results associated with this experimental work have been presented and trends established. A correlation between the basic material property tests and results from the static compression impact tests indicates that the material with the highest interlamina fracture toughness, as obtained from width-tapered fracture specimens, exhibits the greatest residual compression strength in impact-damaged laminates.

Ultrasonic through-transmission inspection and photomicrographs revealed significant differences in the impact-induced fracture modes for different materials. T300/BP907 exhibited the highest resistance to damage, whereas T300/5208 exhibited extensive delamination under identical impact conditions. It has been shown that damage size detected by ultrasonic through-transmission scan is an inaccurate measure of the real damage and is not relatable to residual compression strength. Serious internal damage in the laminate could be present without visible surface damage.

Results of the static compression tests demonstrate that nonvisible damage associated with low-velocity impact in T300/5208 can reduce compression strength to 40% of undamaged strength. Nonvisible damage in T300/BP907 reduced strength to approximately 80% of undamaged strength. Comparison of failure loads for laminates with circular holes, simulated delaminations, and low-velocity impact damage, showed that the severity ranking of those three damage types changed with the different resins. Specifically, impact damage in T300/5208 was more severe than circular holes; in T300/BP907 the converse applied. For both materials the failure loads for circular holes were similar.

Moiré fringe monitoring of specimens under steadily increased compression loading demonstrated delamination growth. Large surface delamination occurred on some simulated delamination specimens, but only minor growth was detected on impact-damaged specimens. Knowing the extent of surface delaminations was insufficient for characterizing reduction in compression strength.

Experimental results from the cyclic compression tests also indicate that impact-induced damage in T300/5208 significantly decreases cyclic life of the laminate. Dynamic photographic recording of moiré fringe demonstrated growth of surface delamination under constant load level cycling. Plots of cyclic strain levels versus cycles to failure for different laminates and types of damage were obtained. Of the three materials evaluated, T300/BP907 exhibited the best overall cyclic compression capability.

Of the types of damage evaluated (circular holes, simulated delamination, and low-velocity impact) the impact-induced damage was the major discriminator on residual compression strength and cyclic compression life.

8.0 RECOMMENDATIONS

The results of this experimental work demonstrate that the resin system is a significant factor in improving residual compression strength and cyclic compression life of laminates with damage incurred during low-velocity impact. Additional evaluation is needed to obtain more data on the behavior of these materials.

- Characterization of internal fracture modes following low-velocity impact and correlation with resulting residual compression strength reduction for selected graphite/polymer systems would provide improved understanding.
- Delamination growth initiation and rates of growth under both steadily increasing compression and cyclic compression need evaluation.
- Improved material screening tests that provide a better measure of interlamina strength, interlamina ductility, and interlamina toughness are acutely needed for these strongly anisotropic laminated graphite/polymer systems.

Results of material evaluation at the laminate level should be introduced at the structural level as well. The tougher acceptable material systems, as verified by laminate tests, could be incorporated into typical wing panel designs. Testing of selected designs would verify whether material response improvements at the laminate level carry over to specific aircraft design configurations. Such configurations introduce the potential for additional failure modes and load redistribution not present at the laminate level. In particular, the influence of stiffeners adjacent to a damaged region is of paramount interest. Continuing developmental effort is necessary to verify the damage containment capability of highly strained composite primary structure.

9.0 REFERENCES

1. Kramer, James J.: Overview of NASA CTOL Program. NASA Conference Publication 2036, pt. 1, pp. 1-7. Proceedings of CTOL Transport Technology—1978.
2. Withington, H. W.: Commercial Air Transportation in the Next Three Decades. Boeing Document D6-46309, Rev. 1, undated.
3. Heldenfels, R. R.: Recent NASA Progress in Composites. NASA TM X-72713, 1975.
4. Dexter, H. Benson: Composite Components on Commercial Aircraft. NASA TM-80231, 1980.
5. Rhodes, M. D.; Williams, J. G.; and Starnes, J. H., Jr.: Low-Velocity Impact in Graphite-Fiber Reinforced Epoxy Laminates. Proceedings of the 34th Annual Conference of the Reinforced Plastics/Composite Institute. The Society of the Plastics Industry, Inc. (New Orleans, Louisiana), 1979.
6. Gause, Lee W.; and Huang, Shih L.: Compression Fatigue of Impact Damaged Graphite/Epoxy Sandwich Beams. NADC-77305-60, 1978.
7. Byers, B. A.; and Stoecklin, R.L.: Preliminary Design of Graphite Composite Wing Panels for Commercial Transport Aircraft. NASA CR-159150, 1980.

Preceding page blank